Development of a design methodology for transonic rotor blades with ORC application

Lucrezia Scalcerle

Delft University of Technology

TU Delft Delft University of Technology

Challenge the future

DEVELOPMENT OF A DESIGN METHODOLOGY FOR TRANSONIC ROTOR BLADES WITH ORC APPLICATION

by

Lucrezia Scalcerle

in partial fulfillment of the requirements for the degree of

Master of Science
in Mechanical Engineering

at the Delft University of Technology,
to be defended publicly on Monday October 30, 2017 at 9:30 AM.

Supervisor:	Dr. ir. Rene Pecnik,	TU Delft
	Ir. Gustavo J. Otero,	TU Delft
Thesis committee:	Prof. dr. ir. Bendiks Jan Boersma,	TU Delft
	Dr. ir. Matteo Pini,	TU Delft
	Prof. dr. ir. Jos van Buijtenen,	Triogen B.V.

TU Delft Delft University of Technology

ABSTRACT

Organic Rankine Cycles (ORCs) are one of the technologies that can play an important role in the reduction of green house emissions. By converting low temperature energy sources in electricity, they are suitable for the exploitation of renewable sources (as solar and geothermal) and industrial waste heat. One of the most critical components in ORCs is the gas turbine, which usually has a radial inflow and one single expansion stage. The difficulties of the turbine design are related to real gas effects of the working fluids (organic compounds) and high expansion ratios, which lead to a supersonic flow at the turbine exit.

The objective of this work is to develop a blade design methodology for a transonic turbine rotor. This is done by setting the focus on the blade passage and shaping it as a rotating nozzle. First, theory of rotating nozzles is developed, assuming the flow to be one dimensional and isentropic. Relations with respect to chocked conditions and the analytic solution to the flow field are derived. Afterwards, the blade design methodology is developed based on the rotating nozzle theory. Inputs of the methodology are total conditions, mass flow and static pressure at the rotor inlet, static pressure at the rotor outlet. Both the theory developed and the blade design methodology are validated. The relations derived for a one dimensional flow through an isentropic nozzle are valid for an ideal gas, while validation for real gas is not carried out. The location of the physical throat and its cross sectional area are determined and the analytic solution method of the flow field is proved to be precise. The blade design methodology is based on a one dimensional approximation and represents a first step towards a more precise blade design: the flow conditions along the nozzle mid line follow the expected trend. However, the boundary conditions are not respected and the flow varies considerably far from the mid line. Additional levels of complexity (as 2D approximation) have to be implemented in future work.

CONTENTS

List of Figures

List of Tables

NOMENCLATURE

Abbreviations

ASM	Analytic solution method
b	Blade
BC	Boundary conditions
CFD	Computational fluid dynamics
err	Percentage error
FVD	Finite volume differences
LE	Leading edge
MOC	Method of characteristics
TE	Trailing edge

Subscripts

θ	Peripheral direction
1	Stator inlet
2	Stator outlet/rotor inlet
3	Rotor outlet
dist	Distribution
H	Hub
in	Inlet
iso	Isentropic
N	Normal component
n	Direction orthogonal to a stream line
out	Outlet
PS	Pressure side
r	Radialθ direction
rel	Relative frame of reference
s	Entropy and direction tangential to a stream line
SS	Suction side
T	Tip
th	Throat
z	Direction orthogonal to the plane (x,y) and (r,θ)

Variables

α	Angle between v and radial direction [deg]
$\bar{\bar{\tau}}$	Stress tensor
$\bar{F}$	Force [N]
$\bar{u}$	Peripheral speed [m s^{-1}]
$\bar{v}$	Velocity in the absolute frame of reference [ms^{-1}]
$\bar{V}'$	Velocity of a rotating frame of reference with respect to the absolute one [ms^{-1}]
$\bar{w}$	Velocity in the relative frame of reference [ms^{-1}]
$\bar{w}^*$	Corrected velocity in the relative frame of reference [ms^{-1}]
$\bar{x}'$	Position of a point in the plane (s,n) [m]
β	Angle between w and radial direction [deg]
δ	Stagger angle [deg]
$\dot{m}$	Mass flow [kgs^{-1}]
$\dot{Q}$	Heat flux [J]
$\dot{W}$	Work [J]
η	Efficiency [-]
γ	Heat capacity ratio [deg]
Λ	Degree of reaction [-]
ω	Speed of rotation [s^{-1}]
Ψ	Stream line
ρ	Density [kg m^{-3}]
{}	Array
F_{in}	Inertia force [N]
f_{in}	Inertia force acting on flow section of length dr [N m^{-1}]
S_h	Energy source term [$Jkg^{-1}K^{-1}$]
A	Cross sectional area [m^2]
A^*	Corrected cross sectional area [m^2]
ang	Angle between the trailing edge of two adjacent blades and the center of rotation [deg]
c	Speed of sound [ms^{-1}]
d	Distance [m]
E	Total energy [$Jkg^{-1}K^{-1}$]
e	Energy [$Jkg^{-1}K^{-1}$]
g	Gravity acceleration [m s^{-2}]
h	Enthalpy [Jkg^{-1}]

h_b	Blade height [m]
H_{tot}	Total enthalpy [Jkg^{-1}]
I	Rothalpy [Jkg^{-1}]
I^*	Corrected rothalpy [Jkg^{-1}]
k_{eff}	Effective thermal conductivity [$(W K^{-1}m^{-1})$]
M	Mach number [-]
N_b	Number of blades in the rotor [-]
p	Static pressure [Pa]
p^*	Critical pressure [Pa]
R	Radius and gas constant [m], [$J\ K^{-1}\ mol^{-1}$]
S_{tot}	Total entropy [$Jkg^{-1}K^{-1}$]
T	Temperature [K]
t	Time [s]
T_{tot}	Total temperature [K]
z	Altitude [m]

ACKNOWLEDGEMENTS

First, I would like to thank my family, that drove me through this important path since the really first day. I am grateful for the trust I received, for never doubting in my capacities and for all the sacrifices they did to let me reach today's dream. The support I received was such a big present that simple words cannot describe my gratitude.

My sincerest thanks go also to my supervisor Dr. ir. Rene Pecnik and to my daily supervisor Ir. Gustavo Rodriguez, who helped me every day in the past nine months. Thanks to their meticulous help and to the long hours spent together, in meetings and discussions, today I can be proud of my work. They have always found the time to drive me through the thesis, to teach me something new and to cheer me up when "the rotor was winning the battle". If I had to start again, I would choose exactly the same team, that now I have to leave with a smile and a hint of sadness.

I am also thankful to Prof. ir. Jos van Buijtenen and Ir. Quirijn Eppinga for giving me the possibility to collaborate with Triogen. Their inputs and friendly help, as much as the application to Triogen's turbine, made me aware of all practical problems related to the turbine design, which as students we tend to forget. Without their collaboration, my thesis would have had a different shape.

I am grateful to the rest of the examination committee, Prof. dr. ir. B.J. Boersma, Dr. ir. Matteo Pini, for dedicating their time to my defense and to read this document.

Finally, I would like to thank all those who, directly and indirectly, helped me out through the past months. I am grateful to Nitish, who has always been available for "turbine related" suggestions. Thanks to my good friends Luca, Bala and Eli, with whom I shared happiness, anxiety, laughs and coffee. I don't want to forget my new friends form P&E: Hirad, Roy and Simone. Also because of them, I came to the office with a smile. Sofi and Laura were sisters to me and, together with Ari, Marta, Ele, Criki, Mary, Melo and Cusco, they supported me from far away; it always helps to know that, wherever you are, you have a place where to go back. At last, thanks to "The Italians". They have been a group, a family, an adventure and so much more... Mentioning each one of them, with no description, would diminish their importance. So I will keep them as a group, knowing that each one of them was unique and gave me the strength to reach the end of my studies.

Lucrezia Scalcerle
Delft, University of Technology
30^{th} October 2017

1

INTRODUCTION

In the past decades, climate changes and the influence of greenhouse emissions became topics of growing importance, to the point that EU set new emissions limits for 2050 and mid targets for 2030. The Paris agreement, signed in 2016, aims to keep the world average temperature rise below $2°C$ with respect to 1990, while $1.5°C$ is considered to be the temperature actually limiting the impact of global worming, [2]. In this scenario, two key issues must be taken into account: the world energy demand is exponentially increasing every year and today's energy sector is mainly fed by fossil fuels, Fig. (1.1). Therefore, to reach the target imposed by Paris agreement it is imperative to move towards an economy based on renewable energy and higher energy efficiency [3].

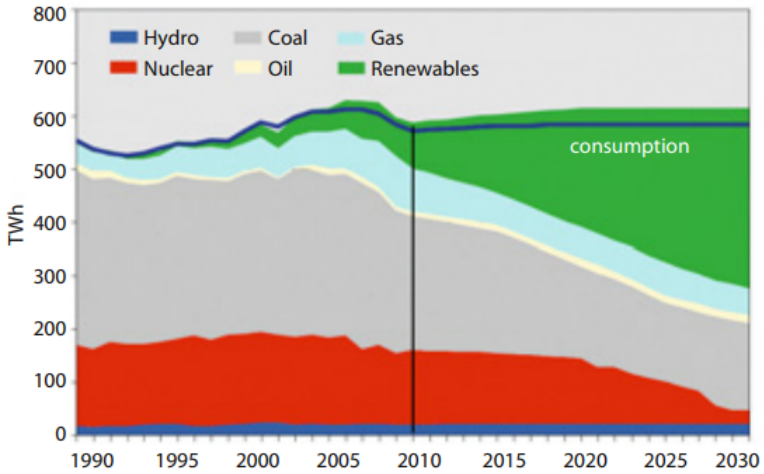

Figure 1.1: Forecast of the sources of the German elecricity production, [4]

However, exploitment of renewable sources comports big challenges, including the fact that often they cannot provide a constant power supply (photovoltaic and wind) or that they provide heat at low temperatures compared to combustion of fossil fuels (solar, geothermal and biomass). Higher energy efficiency in industry can be reached by making use of waste heat, which is usually lost in ambient due to the low temperature of the waste streams. In this scenario, technologies that make use of low temperature heat sources become of particular interest in order to reduce green house emissions. Within these, Organic Rankine Cycles (ORC) represent a good solution both for higher usage of renewable energy sources and for reaching a higher energy efficiency in industrial context. In fact, ORC are used to convert low grade heat into electrical power thanks to the low critical temperature of the working fluid. In the past years the ORC market has been rapidly increasing and this technology is becoming more and more attractive [5]. Research and development in this field is still active, the current thesis is part of a bigger project that focuses of the optimization of turbines for ORC application. The thesis work is carried out in collaboration with the ORC manufacturer Triogen [6],

which provides systems using toluene as a working fluid.

In the introduction chapter general information about ORC cycle are provided. The thesis topic is introduced more into detail, as well as the former work done on it. Finally the thesis outline is given.

1.1. BACKGROUND INFORMATION

1.1.1. ORGANIC RANKINE CYCLE

Organic Rankine cycles are closed thermodynamic cycles that convert heat into work through 4 main steps: compression, heat addition, expansion and cooling. The typical configuration scheme of an ORC is represented in Fig. (1.2b) and does not differ from the basic Rankine Cycle one, Fig. (1.2a). The main difference in between the two is linked to the working fluid, which in ORC cycles is an organic compound rather than water. The advantages of organic compounds with respect to water are due to the main difference in the saturation curves of the fluids [7] and can be easily seen in Fig. (1.3). First of all, in ORC supercritical conditions are reached at lower temperatures, which allows for usage of low temperature heat sources as biomass, solar power, geothermal and waste heat. In addition, the saturation curve of organic compounds has a steep or even negative slope on the liquid-vapour side, which allows for a dry expansion in the turbine. Less turbine stages are required due to the lower enthalpy drop of organic fluids, while the small density changes from liquid to vapour state allow for a compact system [5]. However, the shape of the curve implies also some drawbacks: the low enthalpy difference in between vapour and liquid implies consistently higher mass flows to achieve the same work extraction as with water. Factors as toxicity of the fluid and differences in the plant design have to be taken into account as well.

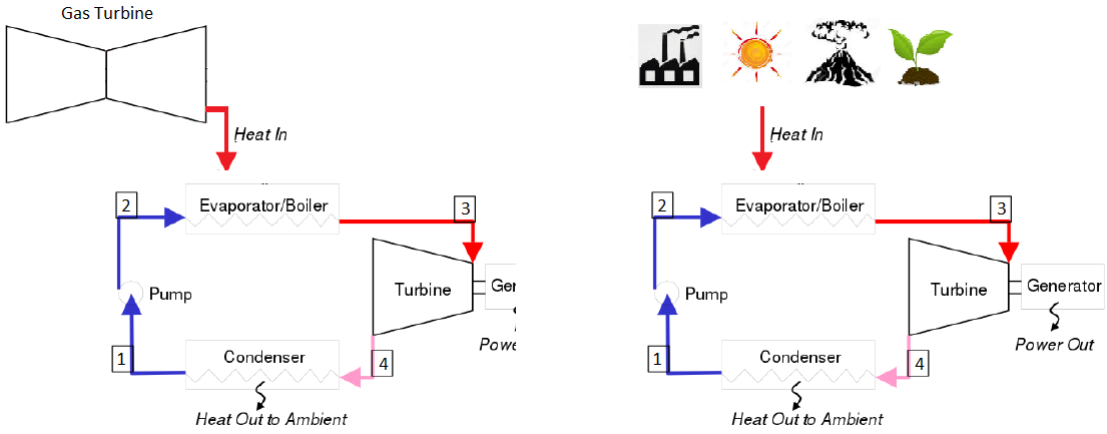

(a) Steam Rankine Cycle

(b) Organic Rankine Cycle, [5]

Figure 1.2: Plant configuration for classic and organic Rankine Cycles

1.1.2. THE EXPANDER - DESIGN APPROACH

One of the most critical components or the ORC configuration is the turbine, which directly influences the performance of the overall system. In fact, the design of turbines for ORC applications implies some main challenges due to the working fluid and to the blade geometry. For example toluene is polyatomic molecule and its properties go through strong variations depending on temperature and pressure [8]. ORCs operate with high pressure ratios, therefore real-gas effects of the working fluid cannot be neglected. In addition, due to the high molecular weight and low speed of sound of toluene, the compound used in the current work, the flow is most likely to reach supersonic conditions when operating with high pressure ratios. Therefore, a non-optimal blade shape is most likely to induce shock waves, leading to big entropy losses and lower efficiency.

ORC applications usually make use of radial inflow turbines. This is due to the several reasons, [9]:

- they allow large enthalpy differences for low peripheral speeds,
- they have a lower sensitivity to blade profile inaccuracy,

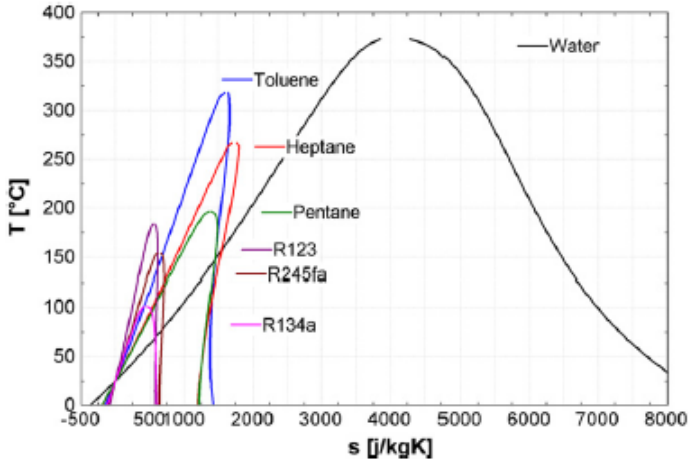

Figure 1.3: Saturation curves of water and organic compounds, [7]

- they guarantee high efficiency at off design conditions,
- they have a higher stability of the rotor and a simpler sealing structure.

However, compared to axial turbines, the design of radial turbines in generally more challenging due to their three dimensional geometry and to the intensity of inertia forces varying along with the flow. According to Zangeneh [10], turbomachinery design can be approached in two different ways, by solving either the direct or the inverse problem. The direct problem consists in determining the shape of the blades and solving the flow in between them through numerical simulation. The improvement of numerical simulation techniques achieved in the past years make the direct approach a valuable and reliable one: a first blade shape is provided and the resulting flow is determined. Afterwards, the shape of the blades is iteratively changed until the desired flow in between the blades is reached. However, the direct approach implies difficulties due to the fact that small changes in the blade shape at any location affect the whole flow field. The problem is particularly important in radial turbomachinery, because of the direction of the flow and of the 3D geometry.

The inverse design method appears therefore to be more suitable: a flow distribution is prescribed and the geometry of the blades is shaped in order to fulfill the requirements. The inverse approach, however, has no control on the shape of the blades, which can result in unrealistic geometries [10]. Few inverse methods were found in literature for 3D flow, all of them implying some limitations. Zangeneh [10] proposes a design method for subsonic compressible flows, while the methods proposed by Ockuroumu and McCune [11], Falcao [12], Tan et Al. [13], Borgers [14] and Ghaly and Tan [15] are all limited to incompressible flows. In addition, it was proven that in inverse method it is impossible to specify pressure/velocity distribution, both on the suction and pressure side, and at the same time to fulfill inlet and outlet BC [16]. Therefore, an approach followed by some authors is to specify properties on the suction side and the blade thickness [10].

1.2. SCOPE AND CONTEXT

From the literature review carried out on the design of radial expanders it was concluded that there is a gap with respect to inverse design methodology. The direct approach is mature, several methodologies base on CFD routines and genetic algorithms were already implemented for blade design and optimization, however such methodologies have high computational costs and provide a limited understanding of the flow. The current thesis work focuses on providing a rotor blade design methodology in between the direct and inverse approach: an initial blade shape is iteratively changed (as in the direct approach) according to a physical model based on the full understanding of the flow (as in the inverse approach).

The expansion in turbines is reached by accelerating the flow in between the blades. When looking at the shape of the stator blades, a nozzle is created in between the suction side and the pressure side of two

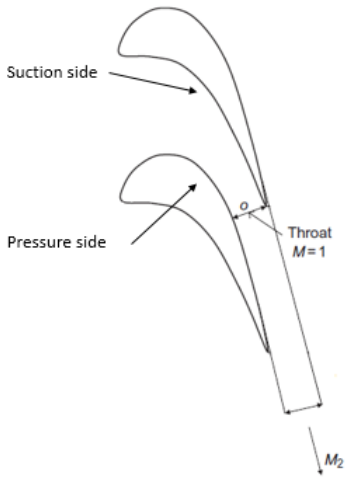

Figure 1.4: Nozzle in between turbine blades, [17]

adjacent blades, as represented in Fig. (1.4). Because of this, the design methodology developed in the current thesis is based on on shaping a nozzle in the blade passage of the rotor. Flows through a static nozzle are known and well described in literature, as explained in Section 2.3.3. However, hardly any literature was found by the author for transonic flows in an inertial frame of reference. A lack of knowledge was found in predicting the throat position and the required cross sectional area to obtain specific flow conditions. Therefore, in order to implement a blade design methodology, a detailed analysis of one dimensional flows through a rotating nozzle is carried out first.

The methodology developed is tested on a real case by proposing a redesign of Triogen's turbine rotor. This choice is due to the optimization process that was already started on the whole turbine. The original turbine design was analyzed in 2012 by means of computational fluid dynamics (CFD) by Harinck et Al. [1]. Several suggestion for the design improvement were given, including:

- a uniform flow should be achieved at the outlet of the stator,
- it would be preferable to increase the speed of rotation to obtain subsonic inlet an increase the power output,
- the rotor should be redesigned to achieve a higher power output. The leading and trailing edge blade angles should be increased.

The stator was recently optimized through the method of characteristics (MOC) by N. Anand, [18], while the redesign of the rotor was started by G. Otero. The main conclusions of his work were used as a starting point for the current work. In particular:

- given the cycle conditions, pressure ratio, shaft speed and wheel diameter, the best possible type of turbine for the Triogen cycle is a radial turbine. This is concluded according the Balje diagrams and the dimensionless parameters of specific shaft speed and specific diameter,
- in the rotor of Triogen's turbine, there must be supersonic conditions as the rotor expansion is grater than the critical one of toluene,
- the rotor stage of the Triogen turbine must be a supersonic blade passage because the expansion is greater that the critical pressure ratio of toluene. It is possible to have a subsonic turbine if the degree of reaction of the turbine is reduced (making the expansion in the rotor smaller) or if the condensation pressure of the cycle becomes larger,

- the area distribution of the original blade passage has the minimal area at the inlet of the rotor, where the sonic conditions are achieved. Moreover, the area distribution shows a sudden decrease near the outlet of the rotor which can produce a shock wave and another sonic conditions in the blade passage.

The optimization methodology proposed by G. Otero was based on exploring a set of geometries and parameters through a genetic algorithm in order to obtain a blade shape [19]. The rotor was considered independently from the stator and the final design resulted in mismatch in between the two components. In the current work the stator is taken into account by setting as inlet boundary conditions the mass flow, the flow velocity and pressure. Design parameters as the degree of reaction and the speed of rotation are changed to achieve more suitable inlet and outlet conditions. Main geometrical parameters, as the inlet and outlet radius and flow direction at the outlet of the stator, are left unchanged. This is done to design a rotor that can actually be integrated in the current system.

1.3. OBJECTIVE AND OUTLINE

In the current thesis, two main objective are pursued; the first one is related to fundamental knowledge upon an expansion through a nozzle in rotation, the second one is related the development of design methodology for radial rotor blades.

First of all, a lack of knowledge was noticed in describing a flow though a rotating nozzle. No literature was found on chocked conditions and on the design of a throat in such a system. Therefore, one of the scopes of the thesis is to reach a deeper understanding of a radial flow expanding in an inertial frame of reference. The aim of the analysis is to be able to design a throat for a specific mass flow and required flow conditions.

The knowledge acquired on the one dimensional flow through a rotating nozzle can be used as a basis for the design of a rotor blade turbine. Therefore, the second objective of the thesis is to develop a design methodology based on an inverse approach. In the thesis work is developed a blade parametrization that relies on a one dimensional flow approximation to generate a three dimensional blade shape. This is meant to be the first step towards a more precise design methodology, where additional levels of complexity are taken into account (as 2D flow approximation rather than 1D).

The structure of the thesis is as follows:

Chapter 2 provides the literature background necessary to fully understand the design methodology. In particular are given a general knowledge on turbomachinery, fluid dynamics and compressible flows. The reader is introduced to the different frames of reference used during the thesis work.

Chapter 3 discusses the theory development for a rotating nozzle. It is considered a one dimensional, isentropic and centripetal flow. For the given system, are derived equations to determine choked conditions and the flow field along the nozzle. The relations derived along the chapter are finally validated.

Chapter 4 provides the blade design methodology developed in the current thesis. A blade parametrization is generated starting from a 1D flow approximation and relying on the relations developed in Chapter 3. The design methodology consists of a preliminary design and of a detailed design, both discussed in the chapter.

Chapter 5 shows the validation of the blade design methodology. It is provided a rotor blade design for Triogen's turbine. The flow field around the obtained shape is simulated through CFD and discussed.

Chapter 6 discusses the final conclusions and recommendations for future work.

2

THEORETICAL BACKGROUND

In order to understand the methodology chosen in the current work, it is crucial to understand the working principle of radial inflow turbines, as well as the physics of the flow through the blades and the forces acting on whole system. In the following chapter the governing equations of turbomachinery and of flows in an inertial frame of reference are introduced. The theory standing behind compressible flows is introduced and it is described the flow through a static de Laval nozzle. The rotor blade design method is developed under several assumptions, which are presented and discussed as well in the current chapter. The aim is to provide sufficient knowledge to understand the methodology adopted in the thesis work.

2.1. RADIAL INFLOW TURBINES

The turbine studied in the current thesis work has a cantilever geometry: the flow is directed inwards through a radial path and is forced thought blades positioned only on the outer region of the rotor, Fig. (2.1). In these turbines, the blades are generally impulsive (with a low degree of reaction); reaction blades can be used as well but they are generally not implemented because they require an increasing cross sectional area, which is difficult to achieve in centripetal turbines, [17]. In Cantilever turbines the flow is not completely deflected in the axial direction, as it happens in classic centripetal turbines; the blade are shaped similarly to axial ones and the radius ratio in between leading and trailing edge is close to unity. In the current work is used the numbering as described in Fig. (2.1):

1. Stator inlet
2. Stator outlet/Rotor inlet
3. Rotor outlet

In the current section are introduced and briefly explained the fundamental turbomachinery relations used during the thesis work. Detailed derivations are explained step by step by S. Dixon et al. [17] and J.P. Buijtenen et Al. [20].

Turbines are machines used to extract the energy from a pressurized fluid and transform it into work by means of an expansion. Given a control volume with an inlet and outlet flow $\dot{m}_2$ and $\dot{m}_3$, a heat addition $\dot{Q}$ and a work extraction $\dot{W}$, as represented in Fig 2.2, the general formulation of the energy equation for a steady flow is given by :

$$\dot{Q} - \dot{W} = \dot{m}\left[(h_3 - h_2) + \frac{1}{2}\left(v_3^2 - v_2^2\right) + g\,(z_3 - z_2)\right], \tag{2.1}$$

where h is the enthalpy, v is the velocity magnitude and z is the altitude with respect to a zero level arbitrarily chosen.

If the flow is assumed to be adiabatic ($\dot{Q} = 0$) and gravity forces are considered negligible ($g = 0$), the specific work can be be expressed by means of total enthalpy drop:

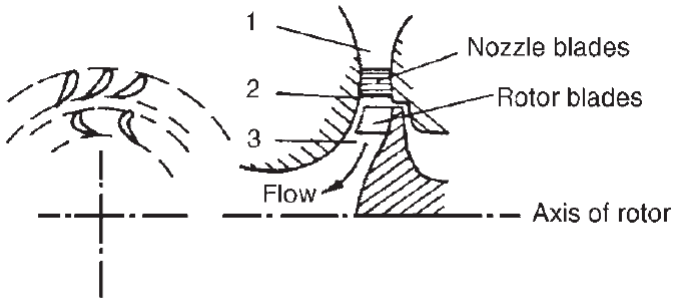

Figure 2.1: Cantilever turbine, [17]

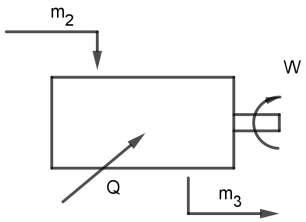

Figure 2.2: Control volume

$$\frac{\dot{W}}{\dot{m}} = H_{tot,2} - H_{tot,3} = h_2 + \frac{1}{2}v_2^2 - \left(h_3 + \frac{1}{2}v_3^2\right). \tag{2.2}$$

In the turbine, two different frames of reference can be defined: an absolute frame of reference, (x, y), and one rotating with the blades, (r,θ). The velocities seen from the two frames are respectively $\bar{v}$ and $\bar{w}$, which are linked by the peripheral velocity $\bar{u}$ through

$$\bar{v} = \bar{w} + \bar{u}. \tag{2.3}$$

The three velocity components, v, w and u can be visualized in vectorial form as triangles; a general velocity triangle and the velocity decomposition in the rotating frame (r,θ) are represented in Fig. (2.3). It is possible to observe that $|\bar{u}| = \omega R$ always has tangential direction, while the radial component of $\bar{w}$ is always the same as $\bar{v}$, therefore $v_r = w_r$. Angles and velocity components can always be derived by means of the system of equations (2.4); angles are measured from the radial direction, α always refers to $\bar{v}$ and β to $\bar{w}$:

$$\begin{cases} w_\theta + u = v_\theta \\ w_s = v_s \end{cases} = \begin{cases} wsin(\beta) + u = vsin(\alpha) \\ wcos(\beta) = vcos(\alpha) \end{cases} \tag{2.4}$$

Velocity triangles play a crucial role in turbomachinery design because they allow to evaluate the flow direction and speed at the inlet and outlet of each stage. In addition, by means of velocity triangles it is possible to define the work done by the fluid also in terms of Euler's equation:

$$\frac{\dot{W}}{\dot{m}} = \left(v_{2,\theta}u_2 - v_{3,\theta}u_3\right). \tag{2.5}$$

Eq. (2.2) and (2.5) can be combined to determine which flow conditions are required at the inlet and outlet of stator and rotor in order to maximize work extraction. Eq. (2.2) tells that the velocity v_3 at the exit of the rotor represents a loss, since the kinetic energy is not converted in work. However, v_3 necessarily has to be different from zero in order to have an outflow from the turbine; a diffuser is often added after the rotor in order to recover the lost kinetic energy. Eq. (2.5) shows that the radial inflow geometry helps work extraction, because the relation $u_2 > u_3$ is always satisfied. It is evident that in order maximize at the same time Euler's

(a) Velocity triangle

(b) Radial and tangential velocity components

Figure 2.3: General velocity triangle and its components in the radial and tangential directions

work and the total enthalpy drop, the velocity v_3 needs to be in the radial direction, therefore $v_{r,3} = 0$; a negative swirl is still beneficial [17].

Eq. (2.2)-(2.5) represent the work that can be ideally extracted by the fluid in an expansion from p_1 to p_3. However, real expansions always involve entropy losses due to irreversibilities, which will be explained later in this chapter. The isentropic efficiency indicates how much of the work ideally available is actually extracted and is expressed by

$$\eta = \frac{h1 - h_3}{h1 - h_{3,iso}}, \tag{2.6}$$

where h_3 is the enthalpy reached in the real expansion and $h_{3,iso}$ is the enthalpy reached in the isentropic expansion. Therefore, the aim of the thesis work to reduce as much as possible entropy losses in order to achieve higher efficiency.

The total expansion in turbine is carried out in two steps: stator and rotor. Work extraction is related to the rotor, Eq. (2.5), while ideally in the the stator it occurs an expansion at constant total enthalpy. If the expansion is isentropic, ($s = const$),two conservation laws can be defined, expressed by (2.7): in the stator the total enthalpy is constant, while the quantity conserved in the rotor in the rothalpy I.

$$\begin{cases} H_{tot} = h + \frac{1}{2}v^2 = const & \text{In the stator} \\ I = h + \frac{1}{2}\left(w^2 - u^2\right) = const & \text{In the rotor} \\ s = const \end{cases} \tag{2.7}$$

Finally, it is possible to quantify the ratio of expansion in the stator and in the rotor by means of the degree of reaction Λ

$$\Lambda = \frac{\Delta h_{rotor}}{\Delta h_{stator} + \Delta h_{rotor}}. \tag{2.8}$$

Since the pressure is described by the equations of state $p = p(h, s)$ and $s = const$, for a fixed p_1 and p_3 different degrees of reaction correspond to different values of pressure p_2. When $\Lambda = 0$ the whole expansion occurs in the stator and the turbine is called impulsive, while if $\Lambda > 0$ it is called reaction turbine and the expansion is shared in between stator and rotor. The relation in between Λ and p_2 can be better seen in Eq. (2.9), where it is clear that for a higher pressure p_2 the difference Δh_{rotor} is higher, and therefore the degree of reaction as well:

$$\Lambda = \frac{h(p_2, s) - h(p_3, s)}{h(p_1, s) - h(p_3, s)}. \tag{2.9}$$

2.2. GOVERNING EQUATIONS

Any flow can be specified by means of conservation laws, where the quantities conserved are namely mass, momentum and energy. These laws can be translated in a set of governing equations describing the flow. The most general formulation of governing equations is given by equations (2.10) - (2.12), [21]

$$\nabla \cdot \rho \bar{v} = 0, \tag{2.10}$$

$$\frac{\partial}{\partial t}\left(\rho \bar{v}\right) + \nabla \cdot \rho \bar{v} \bar{v} + \nabla p = \nabla \cdot \bar{\bar{\tau}} + \rho \bar{F}, \tag{2.11}$$

$$\frac{\partial}{\partial t}\left(\rho E\right) + \nabla \cdot \left(\rho \bar{v} E\right) = \nabla \cdot \left(k_{eff} \nabla T\right) + S_h, \tag{2.12}$$

where ρ is the density, $\bar{\bar{\tau}}$ is the stress tensor, is the absolute velocity, $\bar{F}$ are the volume forces, k_{eff} is the effective thermal conductivity, E is the total energy and S_h is the source term containing the contribution of volumetric heat (e.g. radiation) to the energy equation .

The general set of equations can be consistently simplified by including all the assumptions made on the system. The current work is carried out under the assumption of inviscid and isentropic flow, meaning that all viscosity effects are neglected and that there are no entropy losses along the flow. In addition gravity force is considered negligible compared to the other forces acting on the system (e.g inertia), heat conduction is neglected and the problem is considered to be on steady state.

Some assumption are more or less reasonable than others, therefore in the current section they are commented to evaluate their weight on the final result.

Inviscid flow assumption: this allows to neglect viscous terms in the momentum equation, represented by $\bar{\bar{\tau}}$ in (2.11). Such assumption is largely used in literature as a first flow approximation. The current work aims to be a preliminary study and to provide a first design approach, therefore it is reasonable to initially consider the flow as inviscid. However, it must be kept in mind that by neglecting viscosity, the real problem is not well represented. In fact, wall and turbulent effects play role in the overall flow and they are here not taken into account. Therefore, after a first design it will be important to include viscosity as an additional degree of complexity in the system.

Isentropic flow assumption: this implies that there are no entropy losses in the flow. Entropy in not represented in any of the equations (2.10) - (2.12), therefore an additional equation $s = const$ is necessary to fully describe the problem. Despite the additional equation, such assumption simplifies the problem because it allows for usage of isentropic equations: no prediction of entropy losses is needed. Entropy production is mainly related to viscosity and shock waves; the inviscid assumption removes viscosity as an entropy source, while shock waves will be avoided or reduced by means of the design method.

Negligible body forces and adiabatic system: this allows to neglect gravity forces in the momentum equations and the thermal conductivity and source terms in the energy equation. The forces acting on the system are gravity and inertial forces, which can be calculated as the product in between mass and acceleration: $F = m\,a$. The acceleration of gravity forces is several orders of magnitude smaller than the one due to inertia, therefore the body forces are neglected and the term $\bar{F}$ will include only inertia force. The assumption of adiabatic system allows to remove the terms $\nabla \cdot \left(k_{eff} \nabla T\right)$ and S_h from the energy equation. The adiabatic assumption is reasonable due to the relatively small heat transfer area and to the short time required by the fluid to pass through the turbine [22].

Steady state: this allows to neglect all the $\partial/\partial t$ terms in the governing equations. Such assumption, even in the inertial frame of reference, is not totally true due to the non-uniform flow at the outlet of the stator. However, this unsteadiness can in first approximation be neglected. In order to consider the flow steady state, the set of governing equations has to be modified and expressed in the rotating frame of reference.

Once all the simplifications are done, it is possible to specify the set of equations that fully describes the current problem. It is considered a system rotating steadily with speed of rotation ω with respect to a fixed frame of reference [23]:

$$\nabla \cdot \rho \bar{w} = 0, \tag{2.13}$$

$$\nabla \cdot \rho \bar{w} \bar{w} + \nabla p = -\rho \left(2\bar{\omega} \times \bar{w} + \bar{\omega} \times \bar{\omega} \times \bar{R}\right) = \rho \bar{F}, \tag{2.14}$$

$$\nabla \cdot \left(\rho \bar{w} I\right) = 0, \tag{2.15}$$

$$s = const, \tag{2.16}$$

Equations (2.13)-(2.16) are the ones governing the flow and used for CFD validation. In the current work, the problem is initially approached by representing the space in between blades as a general, rotating nozzle. A 1D analysis is carried out on the mid line Ψ of a rotating nozzle.

2.3. COMPRESSIBLE FLOWS IN A STATIONARY FRAME OF REFERENCE

Gas dynamic is the discipline that studies compressible flows, defined as flows in which pressure-induced changes in density are important. Compressibility effects become of interest when studying high speed flows around an object, including external and internal flows [24]. A direct consequence of compressibility is that the flow allows propagation of waves. Because of this big difference form incompressible regime, compressible flows need to be studied separately. In fact supersonic conditions may be reached, meaning that the fluid is faster than the propagation of sound waves through it. In this case new phenomena arise, such as flow and properties discontinuities. A measure of the speed of the flow compared to the speed of sound is given by the Mach number, defined as

$$M = \frac{v}{c}, \tag{2.17}$$

where c is the speed of sound and depends both on the fluid and on the equation of state $c = c(T, s)$.

Choked conditions are reached when the flow is sonic, therefore $M = 1$. The evaluation of choked conditions, geometry considerations and discontinuities are crucial for a proper design or the rotor: a transonic flow has to be reached and losses need to be as small as possible.

2.3.1. GEOMETRY CONSIDERATIONS AND FLOW CAPACITY EQUATION

For sake of simplicity, while going through geometry considerations, a perfect gas flowing through a stationary and isotropic duct is taken into account. A simple 1D problem is analyzed in terms of mass conservation, expressed in integral form by

$$\dot{m} = \rho A v_N, \tag{2.18}$$

where v_N is the velocity component normal to the cross section A.

The study of the effects of the area on the flow are described step by step by Kundu, [24]. The analysis starts from Eq. (2.19), the differential form of the continuity equation for compressible flows:

$$\frac{d\rho}{\rho} + \frac{dv}{v} + \frac{dA}{A} = 0. \tag{2.19}$$

Such equation expresses the variations of area with respect to variations of velocity and density, which always have to balance in order to guarantee mass conservation. It can be proven that for a compressible, frictionless, adiabatic flow and with no forces acting on the system Eq. (2.20)-(2.21) stand, which combined with Eq. (2.19) allow to write Eq. (2.22):

$$v dv = -\frac{dp}{\rho} = c^2 \frac{d\rho}{\rho}, \tag{2.20}$$

$$\frac{d\rho}{\rho} = -M^2 \frac{dv}{v}, \tag{2.21}$$

$$\frac{dv}{v} = -\frac{1}{1-M^2}\frac{dA}{A}, \tag{2.22}$$

Eq. (2.20) and (2.21) tell that in order to increase the velocity ($dv > 0$) the pressure necessarily has to decrease ($dp < 0$), and that for $M << 1$ density variations are negligible with respect to velocity ones. At $M >> 1$ the opposite statement stands. From Eq. (2.22) it is deduced that in order to increase the flow speed in subsonic regime the area has to decrease, while in supersonic regime it has do increase. Sonic conditions ($M = 1$) are reached in the throat, where the area is minimum.

Such conclusion is well known in literature and it is at the basis of gas dynamics. However, it is crucial for the current work since the main goal is to determine the right area distribution along a streamline. Neglecting the dependency of the area distribution on the Mach number might lead to a completely wrong flow.

The mass flow in a stationary frame of reference can be expressed as a function of the Mach number and of the total quantities p_{tot} and T_{tot}, as shown in Eq. (2.23):

$$\dot{m} = \left(1 + \frac{\gamma-1}{M^2}\right)^{-\frac{\gamma}{\gamma-1}} p_{tot} M \sqrt{\frac{\gamma}{RT_{tot}}} \sqrt{1 + \frac{\gamma-1}{2}M^2}\, A, \tag{2.23}$$

where R is the gas cosntant and γ is the heat capacity ratio of the fluid.

2.3.2. DE LAVAL NOZZLE

From the previous section it is concluded that, given static and isentropic duct with subsonic inlet, the flow accelerates if a convergent section is provided ($dA < 0$). Once the flow reaches sonic conditions, it can further accelerate only if the section is divergent ($dA > 0$). Sonic conditions are reached at the point of minimum area, called throat. Therefore, a transonic flow can be reached only in a convergent-divergent section, which is called de Laval nozzle, Fig. (2.4). However, the presence of a throat does not necessarily imply a transition from subsonic to supersonic conditions. In fact, supersonic conditions are reached only if the total to static pressure ratio at the outlet of the nozzle is below a critical one:

$$\frac{p_{tot}}{p} > \frac{p_{tot}}{p^*}, \tag{2.24}$$

where p^* is the pressure at which the flow would have sonic conditions.

To better explain the concept, Fig. (2.4) is taken into account. The flow before the nozzle inlet has a velocity $v = 0$ and constant total pressure P_t, the back pressure P_b is variable; as soon as $P_b < P_t$, the flow in the nozzle has to speed up in order to match the outlet boundary condition. If $P_b > p^*$ the total to static pressure ratio is lower that the critical one and the outlet boundary condition is matched at a flow speed lower than the sonic one. Therefore the flow speed initially increases, in the throat $M < 1$ and when the divergent section starts the flow velocity drops and the pressure increases; as described by line 2 in figure. When $P_b < P^*$ the flow is necessarily transonic and the expansion depends only on the area, according to Eq. 2.25. However, being the area set, the nozzle might over-expand compared to the pressure boundary condition; in this case a sudden recompression of the flow occurs, line 4 in figure. Section 2.3.3 will refer to such recompression as to a shock wave, however additional details are not needed for the comprehension of the de Laval nozzle. It is concluded that, given a nozzle geometry and the total conditions T_{tot} and p_{tot}, it exists one single back pressure that allows a perfectly isentropic expansion (with no recompressions).

In a stationary de Laval nozzle, the flow conditions at each location can be expressed as a function of the ratio in be between the area at that particular location and the throat nozzle [24]:

$$\frac{A}{A_{th}} = \frac{1}{M}\left[\frac{2}{\gamma+1}\left(1 + \frac{\gamma-1}{2}M^2\right)\right]^{(1/2)(\gamma+1)/(\gamma-1)}. \tag{2.25}$$

It is possible to consider a quasi-1D flow through a nozzle by including the area variation terms in Burger equations:

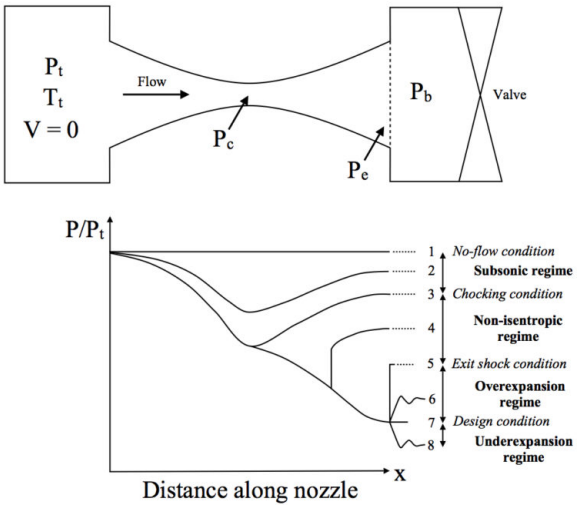

Figure 2.4: Pressure pattern along a nozzole and normal shock wave, [25]

$$\begin{aligned} \text{Mass conservation:} \quad & \frac{\partial \rho}{\partial t} + \frac{(\partial \rho v)}{\partial x} = -\rho v \frac{1}{A}\frac{dA}{dx}, \\ \text{Momentum equation:} \quad & \frac{\partial \rho v}{\partial t} + \frac{\partial (\rho v^2 + p)}{\partial x} = -\rho v^2 \frac{1}{A}\frac{dA}{dx}, \\ \text{Energy equation:} \quad & \frac{\partial \rho E}{\partial t} + \frac{\partial \left(\rho E + p\right) v}{\partial x} = -\left(\rho E + p\right) v \frac{1}{A}\frac{dA}{dx}. \end{aligned} \tag{2.26}$$

2.3.3. DISCONTINUITIES

When dealing with compressibility, discontinuities may occur in the flow. Discontinuities are transition layers where the flow properties go through an abrupt change. Three main flow discontinuities can be identified, namely contact discontinuities, shear waves and shock waves, [26]. In the current section it will be given a general overview on contact discontinuities and shear waves, while a deeper focus will be put on shock waves because of their relevance in the rotor design.

When a contact discontinuity occurs, density, energy and entropy suddenly change across the discontinuity front, while velocity and pressure are constant, as shown in Fig. 2.5a. In shear waves, the velocity component normal to the discontinuity front is constant, while the tangential velocity jumps across the wave, Fig. 2.5b; p, ρ, e, T and s are continuous across the wave.

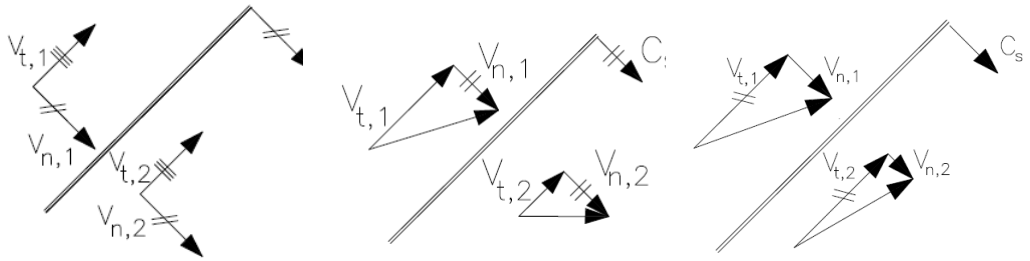

(a) Contact discontinuity (b) Shear wave (c) Shock wave

Figure 2.5: Discontinuities in supersonic flows, [26]

In shock waves, instead, the component of velocity tangential to the wave is constant, while the normal one changes, Fig. (2.5c). In fact, across a shock wave the flow goes through a large pressure rise, which leads

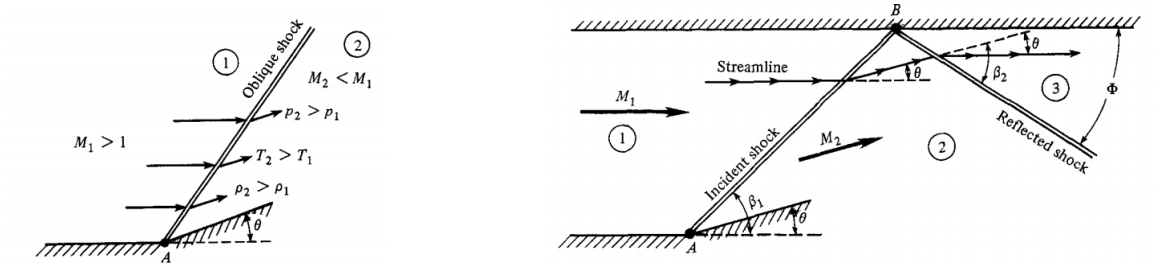

(a) Properties change across an oblique shock (b) Shock reflected on walls

Figure 2.6: Oblique shocks, [28]

to an increase in density. Because of the sudden compression, the process is not reversible and the increase of pressure is balanced by a loss in kinetic energy, which also results in a heating of the gas. Across a shock wave, the gas losses energy and the entropy increases, Zucrow [27]. Because of the entropy increase across the discontinuity, shock waves are responsible for irreversibilities, therefore they have to be avoided as much as possible in the expansion duct. Two main types of shock waves exist: normal and oblique shocks.

Normal shock waves are typical of 1D flows and are always perpendicular to the flow direction. The flow upstream the shock is always supersonic, while downstream it is always subsonic; static temperature, pressure and density increase while the velocity decreases. Normal shocks occur in nozzles when, due to the geometry and to the total conditions, the flow overexpands with respect to the outlet boundary conditions. The sudden flow recompressions mentioned in Section 2.3.2 are oblique shocks, in Fig. (2.4) a shock is represented by line 4.

Oblique shock waves are inclined with respect to the flow direction and they occur when the streamlines are deflected on themselves or when supersonic flows with different speeds are forced to meet. Oblique shocks are generally generated on the leading and trailing edge of blades/wings and in proximity of changes of the flow direction. They may also occur at the exit of nozzles if the pressure boundary condition is not matched, Anderson [28]. Oblique shocks can be of different intensities: "weak shocks" go through a small Δp and they are supersonic, meaning that the Mach number after the shock front is still grater than one. Instead, when a "strong shock" occurs the flow almost instantaneously jumps from supersonic to subsonic conditions, [29]. Therefore, depending on the shock intensity, it is possible to have smaller or grater entropy losses. However, when oblique shocks are incident on walls they generate reflected shocks, that propagate downstream, as represented in Fig. (2.6b). In the entropy loss contribution of an oblique shock also the reflected ones have to be taken into account.

3

THEORY DEVELOPMENT OF ROTATING NOZZLES

As described in Section 2.3.2, one dimensional flows though a static Laval nozzles are already known and well described in literature. Flow conditions are fully determined along the nozzle depending on the boundary conditions, on the throat cross sectional area and on the area distribution; sonic conditions are reached in the throat and the choked mass flow is uniquely determined. The same statements do not hold for a one dimensional nozzle in rotation. In this case, a lack of knowledge was found in predicting the location and the required cross sectional area at which chocked conditions occur.

Due to the little literature found on the topic, in the current chapter a 1D analysis is carried out for a nozzle in rotation. The flow is centripetal and it is analyzed under isentropic assumptions. Initially, a momentum balance is done to understand the influence of the area distribution and of the inertia forces acting on the system. Afterwards, Euler's equations are adapted to the system and a finite volumes solver is implemented to calculate the flow field along a nozzle of a given shape. A graphic methodology is developed to identify the physical throat position and cross sectional area. In addition, an analytic result to the flow field is proposed. The analytic solution methodology and the finite volumes solvers are compared, finally the validation of the theory developed is carried out.

3.1. MOMENTUM BALANCE AND INERTIA CONTRIBUTION

The problem is initially approached by means of a small control volume of length Δr and rotating with angular velocity ω around a point, as described in Fig. (3.1b). A momentum balance is performed on the control volume by following the steps described by Kundu [24] for a nozzle with no speed of rotation; in the current case additional forces acting on the system are taken into account. The analysis is carried out in terms of relative velocity w, therefore the formulation of the momentum equation in integral form reads as:

$$-\dot{m}w_1 + \dot{m}w_2 = p_1A_1 - p_2A_2 + F, \tag{3.1}$$

where the term F represents the body forces acting on the system; in the current case the control volume feels gravity effects and a centrifugal force, however gravity effects are neglected because of a lower order of magnitude with respect to the other forces. Therefore, $F = F_{in}$

If the control volume has differential length dr, as in Fig. (3.1b), the r component of Eq. (3.1) can be written as:

$$\dot{m}\frac{dw}{dr} = -\frac{d}{dr}(pA) + p\frac{dA}{dr} - f_{in} = -A\frac{dp}{dr} - f_{in}, \tag{3.2}$$

$$\rho wA\frac{dw}{dr} = -A\frac{dp}{dr} - f_{in}, \tag{3.3}$$

$$wdw = -\frac{dp}{\rho} - \frac{f_{in}dr}{\rho A}, \tag{3.4}$$

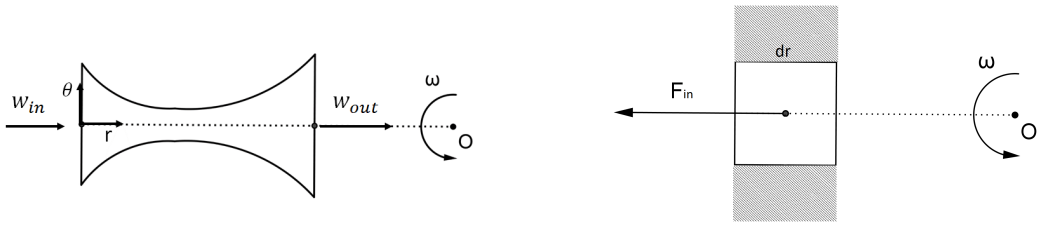

(a) Rotating nozzle with centripetal flow

(b) Control volume in the nozzle

Figure 3.1: Radial inflow nozzle in rotation with respect to a point

where the term f_{in}represents the inertia forces acting on a infinitely small section of nozzle.

By using the speed of sound definition, the term $dp/d\rho$ can be substituted with the term $c^2 d\rho/\rho$. All terms of equation (3.4) can be divided by w^2 to obtain

$$\frac{dw}{w} = -\frac{1}{M_{rel}^2}\frac{d\rho}{\rho} - \frac{f_{in}dr}{\rho A w^2}, \tag{3.5}$$

where M_{rel} is the relative Mach number, defined as $M_{rel} = w/c$.

For sake of simplicity, the term $f_{in}dr/\rho A w^2$ is redefined as K, which is always positive. By means of Eq. (2.19) finally it is obtained

$$\frac{dw}{w}M_{rel}^2 = \frac{dA}{A} + \frac{dw}{w} - KM_{rel}^2, \tag{3.6}$$

$$\frac{dw}{w} = -\frac{1}{1-M_{rel}^2}\left(\frac{dA}{A} - KM_{rel}^2\right). \tag{3.7}$$

Eq. (3.7) is analyzed for the subsonic and supersonic case in the rotating frame of reference:

- for $M_{rel} < 1$, the flow accelerates if $dA/A - KM_{rel}^2 < 1$, therefore for $dA < KM_{rel}^2 A$. It is clear that as long as the relation is respected, the term dA can be both positive or negative, so a convergent section is not strictly needed, as the term kM_{rel}^2 is always positive;
- for $M_{rel} > 1$ the flow accelerates if $dA/A - KM_{rel}^2 > 1$, therefore for $dA > KM_{rel}^2 A$. At supersonic conditions to accelerate the flow speed a divergent area is needed.

From the two previous statements it can be deduced that putting a nozzle in rotation, the sonic point always moves downstream with respect to the throat, but it can never move upstream. The contribution of inertia forces is graphically visible in Fig. (3.2), representing a convergent-divergent section in rotation: it is shown that at the geometrical throat the flow is still subsonic, while the transonic point is located slightly downstream. The sign of each term in Eq. (3.7) is reported and an indicative trend of the quantity dA is plotted in the (r, dA) plane. When the nozzle is in rotation, the curve dA intersects the zero line downstream with respect to $\omega = 0$, the distance in between the two lines is K, as mentioned in Eq. (3.7).

In the current section it was understood that, given a flow through the nozzle, the location of the transonic point can be explained by means of inertia forces. However, it is noticed that such location depends on the term K, which is a function of the flow density and velocity in the relative frame of reference:

$$K = \frac{f_{in}dr}{\rho A w^2}. \tag{3.8}$$

It is concluded that if the flow properties and velocity are unknown along the nozzle, the set of equations provided in the section is not sufficient to identify the throat location.

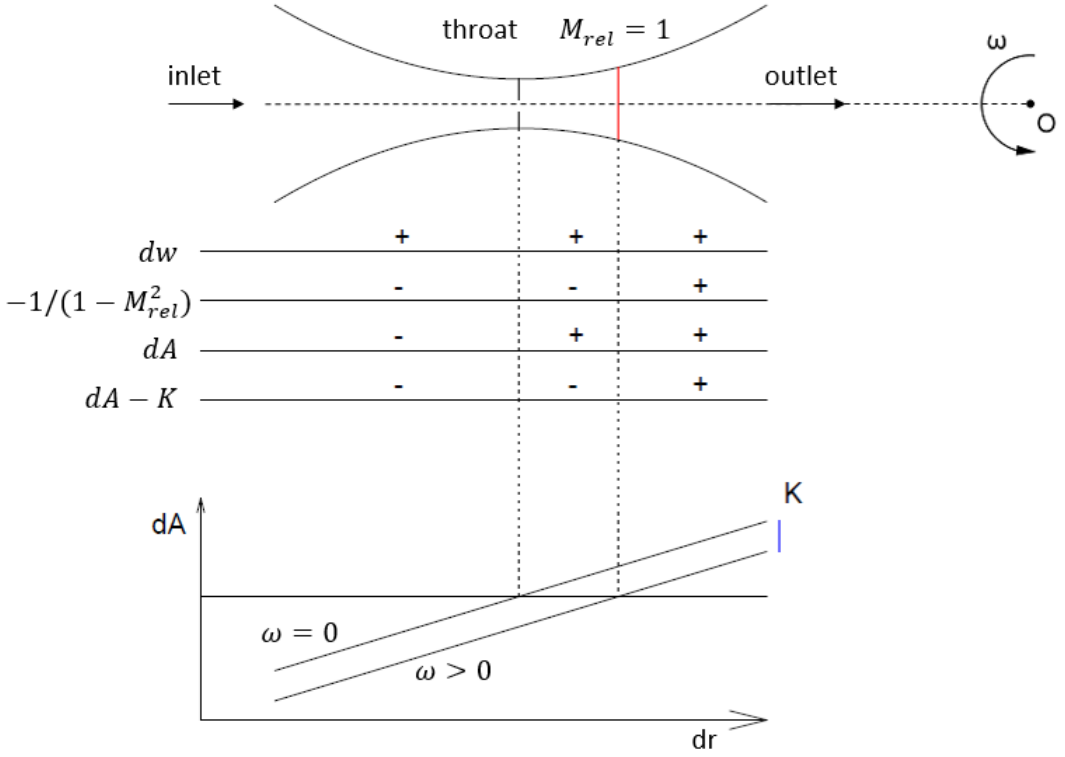

Figure 3.2: Relation in between dw,M,dA and K in a nozzle in rotation

3.2. EULER EQUATIONS IN A ROTATING FRAME OF REFERENCE

In the previous section it was discussed the influence of the inertial term F_{in} on a system in rotation. However, the term was not quantified. In the current section Euler equations are modified to include the inertial term acting on a fluid in rotation. The flow is analyzed in the rotating frame of reference and it is assumed to follow the stream line Ψ in Fig. (3.3). In figure are highlighted the different frames of reference used during the derivation: (x, y) is the absolute frame of reference, (r,θ) and (s, n) are two inertial frames, rotating with speed of rotation ω. The coordinate s is always tangent to the stream line Ψ, while n is orthogonal to it; (r,θ) and (s, n) are define at each location along Ψ.

In the rotating frame of reference, the term v in the quasi-1D Euler equations, Eq. 2.26, is replaced by w. The mass conservation equation is unchanged, while the momentum equation has to include additional terms and the energy equation must be solved in terms or relative total energy. In particular, the additional terms of the momentum equation were derived starting from the general solution described by Kundu [24]:

$$\rho\left(\frac{D\bar{u}}{Dt}\right) = -\nabla p + \rho\left[\bar{g} - \frac{d\bar{V}'}{dt} - 2\bar{\omega}\times\bar{w} - \frac{d\boldsymbol{\omega}}{dt}\times\bar{x}' + \bar{\omega}\times\left(\bar{\omega}\times\bar{x}'\right)\right], \tag{3.9}$$

where $\bar{w}$ is the velocity in the rotating frame (s, n), ω is the speed of rotation of (s, n) with respect to (x, y), $\bar{V}'$ is the velocity of the rotating frame of reference with respect to the fixed one and $\bar{x}'$ is the position of a point expressed in (r, s) coordinates.

For an simpler analysis, the focus is set only on the terms into squared brackets, representing the body forces acting on the system. All terms are considered one by one, taking into account that gravity forces are negligible. Before doing so, however, it is useful to define transformation (3.10), which allows to switch from the coordinate system (r,θ) to the (s, n) one:

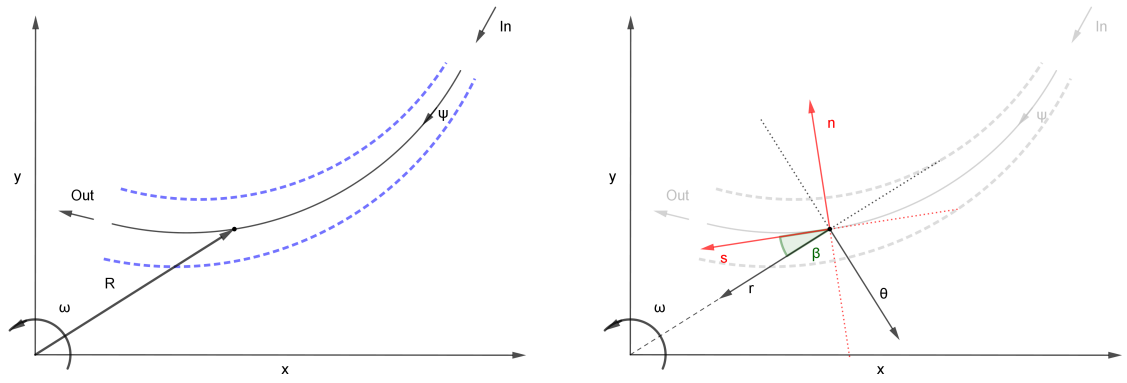

(a) Generic nozzle in rotation

(b) Frames of reference

Figure 3.3: Transonic area distribution - case a-transonic

$$\begin{aligned} \hat{e}_s &= cos\beta\hat{e}_r - sin\beta\hat{e}_\theta \\ \hat{e}_n &= -sin\beta\hat{e}_r - cos\beta\hat{e}_\theta \end{aligned} \tag{3.10}$$

being β the angle between $\hat{e_r}$ and $\hat{e_s}$.

Term 1: To evaluate the term $d\bar{V}'/dt$ it is easier to first reason in terms of the system (r,θ) and to shift afterwards to (s,n). The term can be written as in Eq. (3.11), where R is the distance in between (s,n) and (x,y) (it is recalled that the frame (s,n) is redefined at each location along Ψ). The second derivative can be executed in two steps, through equations (3.12)-(3.13).

$$\frac{d\bar{V}'}{dt} = \frac{d}{dt}\left(\frac{d\bar{R}}{dt}\right), \tag{3.11}$$

$$\frac{d\bar{R}}{dt} = \bar{\omega}\times\bar{R} = -\omega R\,\hat{e}_\theta, \tag{3.12}$$

$$\frac{d}{dt}\left(\frac{d\bar{R}}{dt}\right) = \omega\times(-\omega R\,\hat{e}_\theta) = \omega^2 R\,\hat{e}_r. \tag{3.13}$$

In the coordinate system (s,n), by using the transformation (3.10)

$$\boldsymbol{\omega}\times\left(\bar{\omega}\times\bar{R}\right) = \left(\omega^2 R\,cos\beta\right)\hat{e}_s + \left(-\omega^2 R\,sin\beta\right)\hat{e}_n. \tag{3.14}$$

Term 2: The second term is evaluated directly in the frame of reference (s,n). The flow is assumed to be one dimensional in the direction of the mid line, therefore $w(s,n) = (w,0)$, while $\omega = (0,0,\omega)$. Therefore, the second term reads as in Eq. (3.15) - (3.16):

$$2\left(\bar{\omega}\times\bar{w}\right) = 2\left[\left(-\omega w_n\right)\hat{e}_s + \left(\omega w_s\right)\hat{e}_n\right], \tag{3.15}$$

$$2\left(\bar{\omega}\times\bar{w}\right) = \left(2\omega w\right)\hat{e}_n. \tag{3.16}$$

Term 3: The flow is assumed to rotate with a constant speed of rotation, therefore

$$\frac{d\bar{\omega}}{dt}\times\bar{x}' = 0.$$

Term 4: The frame of reference (s,n) "follows the flow", therefore it is redefined in each point along the nozzle. It follows that the distance of each point along the mid line and the center of the frame of rotation is always zero: $\bar{x'}=0$, meaning that the whole fourth term is null.

$$\bar{\omega}\times\left(\bar{\omega}\times\bar{x'}\right)=0.$$

Terms 1-4 are finally put together in Eq. (3.17) to obtain the additional source terms to the momentum equation in the frame of reference (s,n), body forces are negligible compared to the other forces acting on the system.

$$\begin{aligned}\hat{e}_s \text{ direction: } &\rho\left(-\omega^2 R cos\beta\right)\\ \hat{e}_n \text{ direction: } &\rho\left(-2\omega w+\omega^2 R sin\beta\right).\end{aligned} \tag{3.17}$$

Terms 3.17 are the additional inertial terms that have to be included in the momentum in an inertial frame of reference. Therefore, it is achieved the final set of equations:

$$\begin{aligned}\text{Mass conservation:}\quad & \frac{\partial\rho}{\partial t}+\frac{(\partial\rho w)}{\partial s}=-\rho w\frac{1}{A}\frac{dA}{ds},\\ \text{Momentum equation:}\quad & \frac{\partial\rho w}{\partial t}+\frac{\partial(\rho w^2+p)}{\partial s}=-\rho w^2\frac{1}{A}\frac{dA}{ds}-\rho\omega^2 R\,cos\beta,\\ \text{Energy equation:}\quad & \frac{\partial\rho E_{rel}}{\partial t}+\frac{\partial\left(\rho E_r+p\right)w}{\partial s}=-\left(\rho E_{rel}+p\right)w\frac{1}{A}\frac{dA}{ds},\end{aligned} \tag{3.18}$$

where s is the position along the mid line Ψ, R is the distance of each point of along the nozzle from the center of rotation and the energy equation is written in terms of the relative internal energy:

$$E_{rel}=e+\frac{1}{2}\left(w^2-u^2\right), \tag{3.19}$$

$$E_{rel}=h-\frac{p}{\rho}+\frac{1}{2}\left(w^2-u^2\right). \tag{3.20}$$

The set of equations (3.18) was included in a finite volumes solver, which evaluates a steady state flow through a nozzle in rotation. This was implemented by modifying a code originally written for the static case, it uses a Runge-Kutta Scheme and fluxes are calculated through AUSM [30].

3.3. DETERMINING CHOKED CONDITIONS

In a static nozzle, chocked conditions can be easily determined my means of the flow capacity equation, Eq. (2.23), which at given total conditions and $M=1$ is fully specified. The same equation cannot be used in a rotating frame of reference, where the total conditions are not constant due to work extraction, meaning that Eq. (2.23) is under specified. Therefore, the present section focuses in determining chocked conditions in a rotating nozzle.

A one dimensional and isentropic flow through a nozzle is taken into account; due to rotation, the total conditions along the nozzle are not constant, however conservation of rothalpy I can be taken into account. Therefore, the problem can be fully described by means of the system of equations (3.21), stating that rothalpy, entropy and mass flow in the rotor are constant:

$$\begin{cases} I=h+\frac{1}{2}\left(w^2-u^2\right)=const\\ s=const\\ \dot{m}=\rho A w\end{cases} \tag{3.21}$$

Along a nozzle of a given length, the peripheral velocity $u=\omega R$ is known at each location. Assuming to have some imposed boundary conditions, the terms I, s and $\dot{m}$ are considered to be initially set. System (3.21) is analyzed graphically by rearranging the equations as in Eq. (3.24)-(3.23) and by plotting function (3.24):

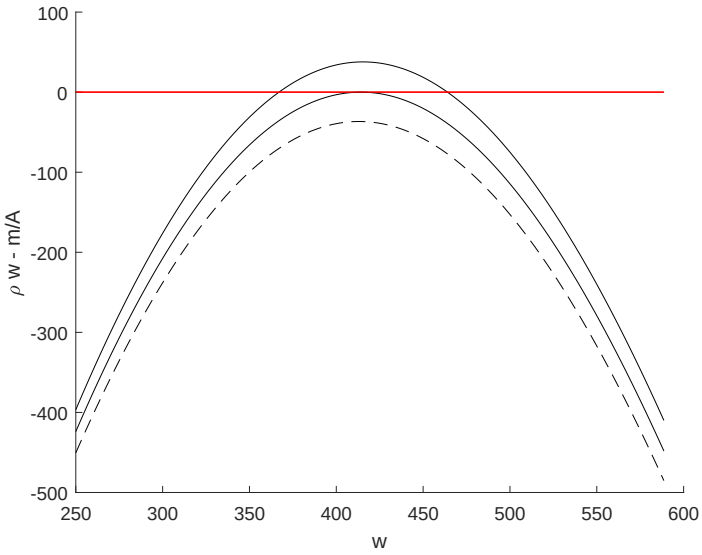

Figure 3.4: Possible curves and solutions

$$h = I - \frac{1}{2}\left(w^2 - u^2\right), \tag{3.22}$$

$$\rho = \rho(s, h), \tag{3.23}$$

$$f(w, u, A) = \rho w - \frac{\dot{m}}{A}. \tag{3.24}$$

In Fig. (3.4) the function $f(w,u,A) = \rho w - \frac{\dot{m}}{A}$ is plotted three times for different input values of A and u, the values are not reported with the purpose to focus only on the shape of the curve and on its position with respect to the zero line (in red). It is recalled that the value of u indirectly influences the curve $f(w,u,A)$ by means of Eq. (3.22)-(3.23). It is noticed that the three curves have the same concavity and the maximum point is located at different distances from the zero line. The intersections of the function with the zero line represent the solutions to system (3.21), which is consistent both with an isentropic flow and mass conservation. Therefore, the graphical method is based on studying the relative position in between $f(w,u,A)$ and the zero line depending on the values of A and u.

In the current work the rothalpy value is always calculated at the inlet of the rotating nozzle, assuming the values of inlet relative velocity w_{in}, enthalpy h_{in} and entropy s to be constant. Once a certain speed of rotation ω is set, the rothalpy I is constant along the nozzle, however for different values of ω impose different values of I. Depending on the input values, three different cases can be distinguished, as in Fig. (3.4):

- the curve $f(w,u,A)$ has two different intersections with the zero line, therefore two different solutions are possible. One of the two solutions is subsonic, the other one supersonic; the conditions of the flow depend on the back pressure and on the boundary conditions,
- the curve does not intersect the zero line, therefore no isentropic solution to system (3.21) is possible,
- the curve has one single intersection, therefore the flow is sonic and at choked conditions.

As previously stated, the possible solutions to the system are hereby analyzed in terms of peripheral velocity u and area A. In order to carry out the analysis, the values of rothalpy, entropy and mass flow necessarily have to be set. The values used in the current work are reported in Tab. (3.1), the fluid used is air. Such values are reported for sake of completeness, however the analysis is general and the conclusion presented later on in the chapter are assumed to be independent on the given values.

Table 3.1: Input values for velocity/area relation analysis

I	[kJ/kg]	$4.427 \cdot 10^5$
s	[kJ/kgK]	$6.674 \cdot 10^3$
$\dot{m}$	[kg/s]	2.000
R	[m]	$0.140 - 0.340$
ω	[1/s]	1100

Influence of area A at constant peripheral velocity u: firstly it was considered the case in which the peripheral velocity u is set to be constant, therefore $f(w,u,A) = f(w,A)$. A location i along the nozzle is chosen and at $R = R_i$ three different areas A_a, A_b and A_c are evaluated, being $A_a > A_b > A_c$; the curves $f(w,A_a)$,$f(w,A_b)$ and $f(w,A_b)$ are plotted in Fig. (3.5a). It is noticed that for $A = A_a$ Eq. (3.24) has two solutions, for $A = A_b$ there is one single intersection while for $A = A_c$ there is no intersection with the zero line, meaning that for the specified values of $\dot{m}$, I, u and A_c an isotropic expansion cannot be reached. It is clear that by decreasing the area, the flow gets closer to sonic conditions, till a minimum area is reached. When $A = A_b$ the flow is choked and smaller areas are not capable of allowing the specified mass flow. Therefore if $A < A_b$ the system admits solutions only for lower mass flows. Such result is important because it allows to define a physical throat where sonic conditions are reached; further in this chapter it will be explained that the physical throat does not necessarily coincide with a geometrical one. As well, given an area distribution and a peripheral velocity u at one location along the nozzle, the choked mass flow can be uniquely determined.

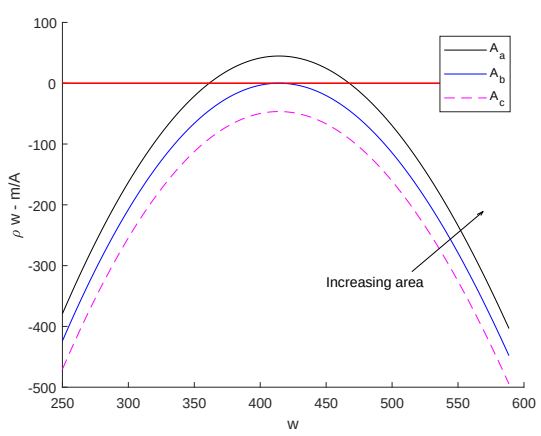

(a) $f(w,A)$ for different values of A at location $R = R_i$

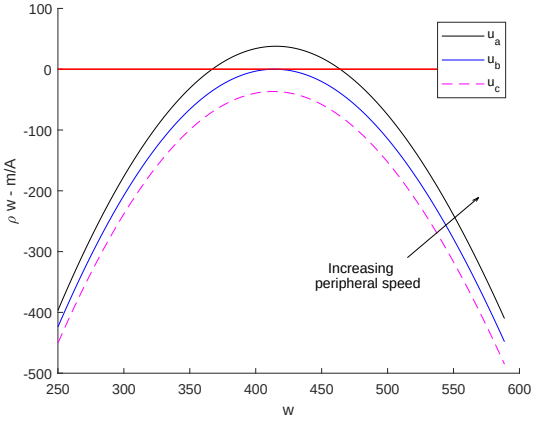

(b) $f(w,u)$ for different values of $u = \omega R$ at a fixed area $A = A_j$

Figure 3.5: Plots of $f(w,A,w)$ depending on the area A and peripheral speed u

‘

Influence of the peripheral velocity u at constant area A: in this case the analysis is carried out assuming to have a constant area $A = A_j$ at different peripheral velocities, therefore $f(w,u,A) = f(w,u)$. Since $u = \omega R$, velocity variations can be related either to different speeds of rotation at a constant location along the nozzle, or to different locations R at a constant speed of rotation. In Fig. (3.5b) it is shown that for $A_j = const$ the solutions to system (3.21) get closer to sonic conditions for lower values of u. The problem can be further split in the two cases of speed of rotation and radius variations:

- if $\omega = const$ and R varies, a centripetal flow accelerates for $M_{rel} < 1$ and decelerates for $M_{rel} > 1$,
- if ω varies and $R = const$, the flow is faster for lower speeds of rotations and it slows down if the speed of rotation increases.

.

It is underlined that the current analysis is carried out for a constant value of rothalpy I. As previously explained, if the flow conditions are imposed at the inlet/outlet of the nozzle, different speeds of rotation set different values of I. Therefore, the second statement applies only to a system in which the inlet/outlet flow conditions are hypothetically adapted to ω in order to maintain $I = const$.

By looking at Fig. (3.5b) it is clear that for $A_j = const$, the maximum of the curve $f(w,u)$ moves to lower values for lower values of u. Two specific cases of $u_b = \omega R_b$ and $u_c = \omega R_c$ are taken into account: at location R_b the function $f(w,u_c)$ has one single intersection with the zero line, meaning that the flow is choked. The same area A_j however at location R_c does not allow any isentropic solution and choked conditions are reached for $A \neq A_j$. An important conclusion of this analysis is that in a rotating nozzle the area of the physical throat depends on the location R_i along the nozzle, therefore $A_{th} = A_{th}(R)$. This represents a main difference with respect to the static de Laval Nozzle, where the location of the throat along the nozzle has no influence on the choked conditions.

SONIC LINE

One of the objective of the present chapters is to be able to identify a throat location and cross sectional area along the nozzle. It was previously concluded that the throat area varies in function of the distance R from the center of rotation, therefore the focus is now set on determining the relation in between A_{th} and R.

This is done by solving system (3.21) at each location R_i along the nozzle and finding the area $A_{th,i}$ for which $M_{rel,i} = 1$. It is followed the algorithm described in Fig. (3.6): the nozzle length is discretized in N elements and a range of velocities $\{w\}$, discretized in K elements, is taken into account. At each location R_i, the enthalpy array $\{h\}$ and the speed of sound array $\{c\}$ are calculated for each value of $\{w\}$. Sonic conditions are reached when $\{w(j)\} = \{c(j)\}$; therefore the throat area is calculated by mass conservation for $\rho_i = \rho(\{h(j)\}, s)$ and $w_i = \{w(j)\}$.

Once the throat area is calculated at each location i, a line is plotted in the plane (r, A), Fig. (3.7). The current work refers to this line as to the "sonic line", which is the locus of points along the axis r having $M_{rel} = 1$. If at any location i along the nozzle the cross sectional area is below the sonic line, the system doesn't allow for isentropic solutions. If the area distribution always lays above the sonic line, an isentropic flow is possible.

In Fig. (3.8) are reported three different sonic lines, calculated at three different speeds of rotation for a constant relative velocity w_{in} at the inlet. Along each curve the rothalpy is constant, but due to the fact that I is imposed at the inlet on the nozzle, the three sonic lines depend on different values of rothalpy. From the figure it is evident that higher speeds of rotation imply higher throat areas.

AREA DISTRIBUTION

It was stated that at a fixed location i along the nozzle, isentropic solutions to system (3.21) are possible only if $A > A_{th,i}$. Therefore, it is concluded that for given values of rothalpy, entropy and mass flow, an isentropic expansion can be reached only if the area distribution on the nozzle always lays above the sonic line. Some considerations are made with respect to the possible area distributions. The inlet and outlet area of the nozzle are maintained constant, the mass flow is imposed and the inlet conditions are subsonic. The choice of setting a mass flow is due to the fact that later on, the model is meant to represent the channel in between the blades of a rotor, where the mass flow is imposed upstream by a choked stator. In Fig. (3.9) are evaluated three different area distributions connecting the inlet and outlet area. The focus is set on the velocity and relative Mach number profiles along the nozzle depending on the path. The flow properties are calculated imposing mass, rothalpy and entropy conservation, while no pressure conditions are imposed at the inlet/outlet of the nozzle. The solution method used will be explained in detail in Section 3.4. Path_a and Path_b are chosen so to touch the sonic line in one point, while the area distribution described by Path_c always lays above the sonic line.

Case a - the area distribution touches the sonic line: Both the area distributions described by Path_a and Path_b touch the sonic line in one point, meaning that a physical throat is provided and that at that location the flow reaches $M_{rel} = 1$. The two area distributions differ from each other for the presence of a geometrical throat. In Path_a in fact the cross sectional area is always diverging, such result is in line with what stated in

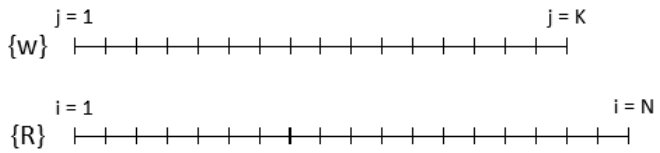

{w}: array of K elements

{R }: array of N elements

for i = 1:N

$$u_i = \omega R_i$$
$$\{h\} = I - \frac{1}{2}(\{w\}^2 - u_1^2)$$
$$\{c\} = c(\{h\}, s)$$
Find j @ $\{c(j)\} = \{w(j)\}$
$$h_i = \{h(j)\}\,; w_i = \{w(j)\}\,;\ \rho_i = \rho(h_i, s)$$
$$A_{th,i} = \frac{m}{\rho_i w_i}$$

end

Figure 3.6: Algorithm for sonic line calculation

section (3.1) and allows for a more flexible shape of the nozzle compared to the static case. In fact, depending on the geometry requirements, a geometrical throat can be provided or not.

Case b - the area distribution does not touch the sonic line: The area distribution described by $Path_c$ is always above the sonic line. A geometrical throat is provided, therefore the flow initially accelerates and then decelerates without reaching sonic condition at any location of the nozzle.

To conclude, through the analysis presented in current section it was possible to have a better understanding of the flow in a rotating nozzle and to identify some physical constrains to the system. Such constrains necessarily have to be taken into account during the nozzle design process. In particular, the following statements can be done for constant values of rothalpy, entropy and speed of rotation:

- choked conditions do exist in a rotating nozzle, there is a maximum mass flow that the nozzle can allow for an isentropic expansion,
- the physical throat can be located anywhere along the nozzle; its value, however, depends on the distance R form the center of rotation. Higher peripheral speeds imply smaller physical throats,
- for a given mass flow, transonic conditions can be reached only if the nozzle is designed to have a physical throat,
- the physical throat does not necessarily coincide with a geometrical throat. A geometrical throat does not lead to sonic conditions unless it is also a physical one.

Such conclusions provide knowledge enough to design the physical throat of a rotating nozzle for a given mass flow and radius. The speed of rotation and the inlet (or outlet) boundary conditions have to be specified in order to set a the rothalpy and entropy to be conserved along the nozzle.

3.4. 1D FLOW THOUGHT THE NOZZLE

In Section 2.3.2 it was explained that for given total conditions and area distribution, the flow conditions along a static nozzle are fully determined by means of Eq. (2.25), therefore $v = v(T_{tot}, p_{tot}, A/A_{th})$. Due to

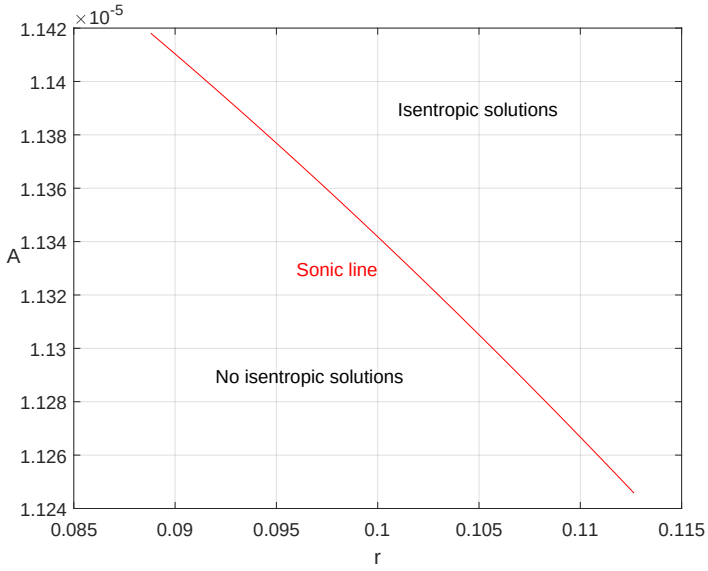

Figure 3.7: Sonic line and regions of the plane admiting isentropic solutions

work extraction, Eq. (2.25) cannot be used in the case of a rotating nozzle, therefore it is looked for a similar relation in between the flow conditions and other imposed conditions. In the present section the system of equations (3.21) is used to directly relate the flow conditions along the nozzle to the area distribution, mass flow, rothalpy and peripheral velocity, therefore $w = w(I, \dot{m}, u, A)$.

It is taken into account a flow at fixed values of $\dot{m}$, I, s, ω and geometry A_{dist}. It is considered a location i along the nozzle, having radius R_i and cross sectional area A_i. For the given boundary conditions, the curve of isentropic solutions for $A = A_i$ has two different intersections with the zero line, being one subsonic and the other one supersonic, Fig. (3.10). The choice of the right solution is done according to the relative position of the point with respect to the throat and depending on the back pressure:

- if location i is upstream with respect to the throat, the flow is subsonic,
- if location i is downstream with respect to the throat and the outlet pressure is above the critical one, the flow is subsonic,
- if location i is downstream with respect to the throat and the outlet pressure is below the critical one, the flow is supersonic.

The concept of such solution method is extremely simple and it allows to solve the flow analytically. This represents a big advantage in terms of computational time and convergence problems. However, the method is not flexible and depends very much on the input values of mass flow, rothalpy and entropy. If these values are not well predicted, the solution provided is wrong. In fact, in reality mass flow, rothalpy and entropy are not imposed and depend on the boundary conditions of the system.

3.5. COMPARISON IN BETWEEN ANALYTIC SOLUTION AND FINITE VOLUMES SOLVER

In the present chapter it was concluded that the flow properties a long a nozzle can be calculated according to two different approaches: either by solving the system of equations (3.21) or by solving Euler equations (2.26). The first approach provides an analytic solution, while the second one relies on finite volumes.

The two approaches are conceptually different and may be used with different purposes. This is due to the different boundary conditions used as inputs for the two methods. In Tab (3.2) are resumed all the inputs and governing equations of the two methods.

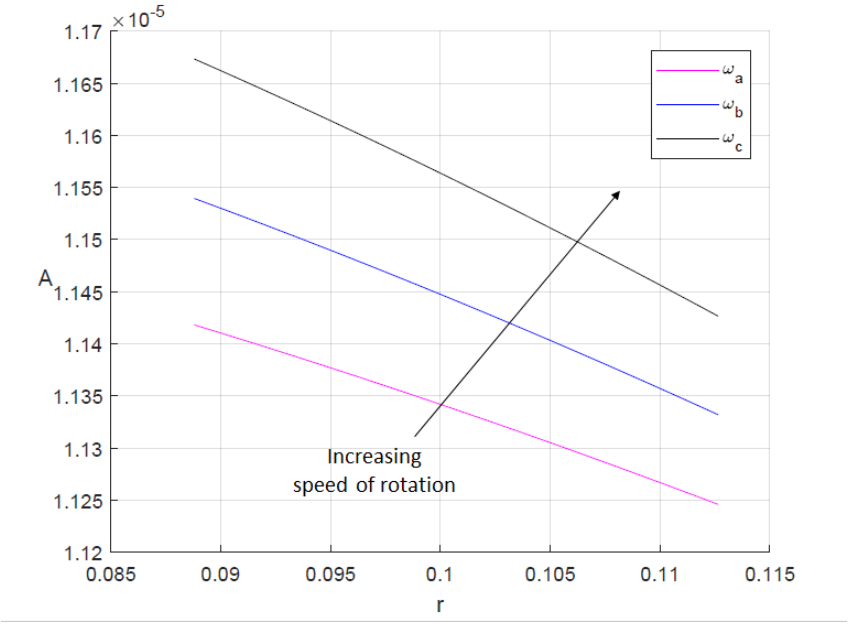

Figure 3.8: Sonic line depending on radius and speed of rotation

Analytic Solution Method (ASM): the solutions depend on the input values of mass flow, rothalpy, and entropy. ASM can be used to design a nozzle for specified flow conditions and mass flows, in this case it is used for inverse engineering. However, it cannot be practically used to evaluate a flow through a given geometry. In fact, the solution ignores the pressure boundary conditions and relies on the specified value of mass flow. In a real case the flow solution and the mass flow thought the nozzle depend on chocked conditions.

Finite Volumes Solver (FVS): the solution depends on the inlet total conditions and on the pressure boundary conditions. The outlet pressure is an input but in only determines whether if the flow at the outlet is subsonic. In the supersonic case, all flow conditions downstream with respect to the flow are independent on the upstream conditions and the outlet pressure boundary condition is not necessarily matched. The mass flow depends on the choked conditions at the throat and cannot be imposed. The finite volumesolver is used to determine the flow conditions through a given geometry, while it cannot be used for inverse engineering.

Table 3.2: System and solver inputs and governing equations

	analytic solutio method (ASM)	**finite volumemethod (FVM)**
Inputs	Geometry	Geometry
	Speed of rotation	Speed of rotation
	Mass flow	Inlet total conditions
	Rothalpy	Outlet pressure
	Entropy	-
Governing equations	Mass conservation	Mass conservation
	Entropy conservation	Momentum equation
	Rothalpy conservation	Energy equation

3.6. VALIDATION

The validation of developed theory is done by using the sonic line to design a nozzle with a specified mass flow and chocked conditions. The inlet and outlet cross sectional area of the nozzle are determined by means of mass, rothalpy and entropy conservation. Afterwards, the flow conditions through the nozzle are calculated by means of the finite differences solver (FVS) and it is verified if the imposed mass flow and boundary

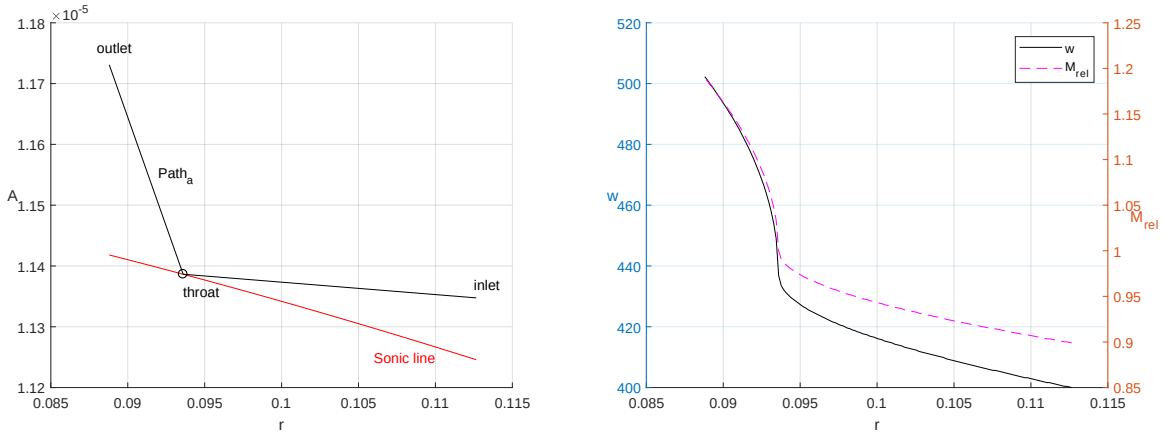

(a) $Path_a$: a physical throat is provided, while no geometrical throat is present

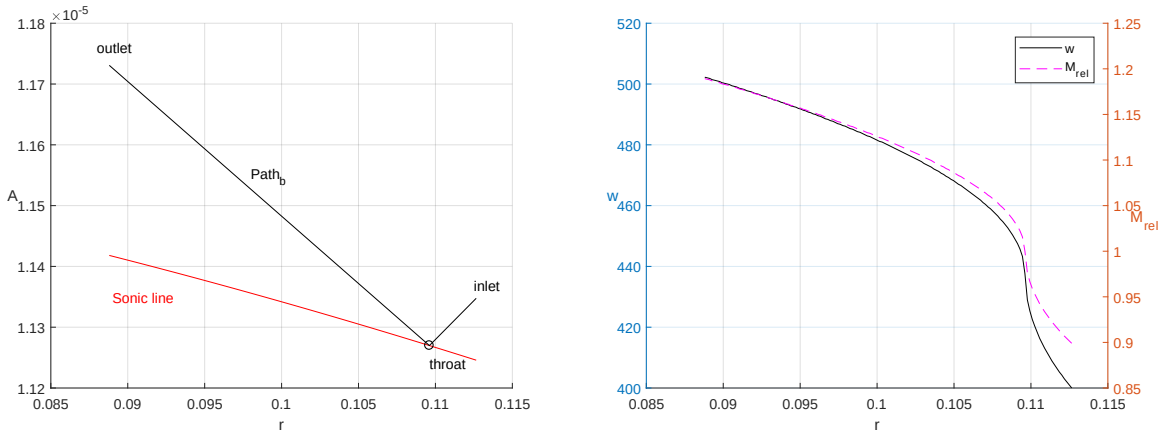

(b) $Path_b$: a physical throat is provided and coincides with the geometrical throat

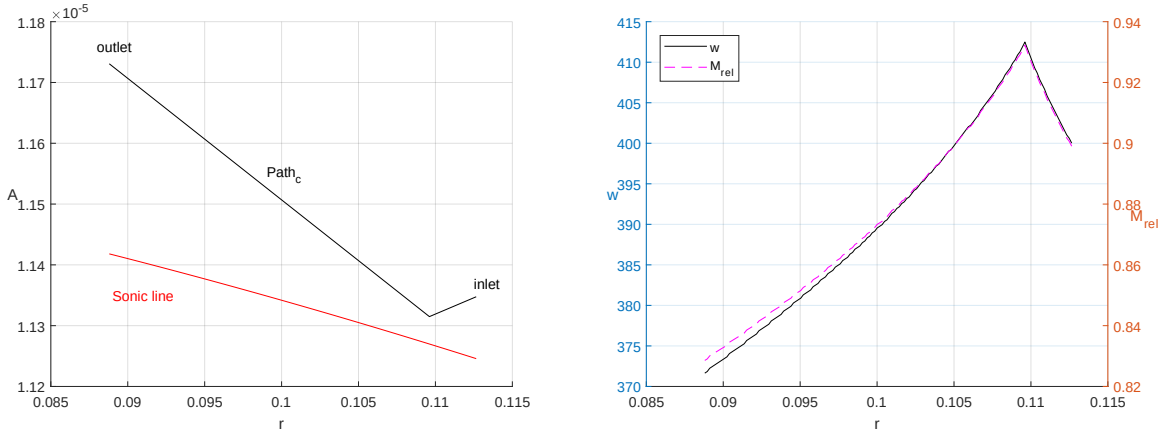

(c) $Path_c$: no physical throat is provided, while a geometrical throat is present

Figure 3.9: Relative velocity and mach number depending of the area distribution

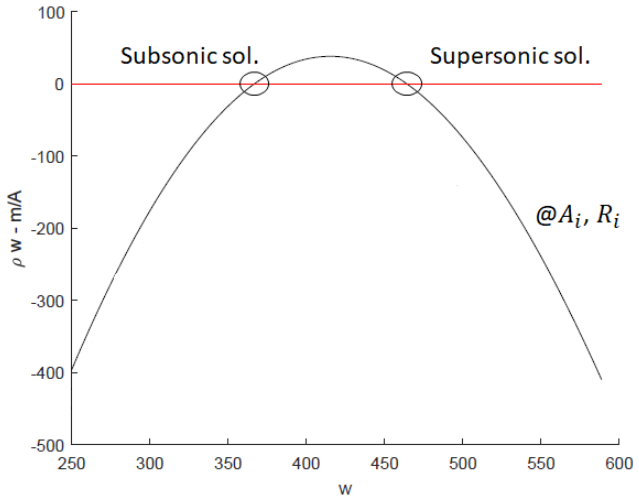

Figure 3.10: Solutions to system (3.21) at location i

conditions are respected. The analytic solution method is validated by calculating the flow conditions along the nozzle by means of ASM and comparing the results to the ones obtained by FVS.

3.6.1. DESIGN OF THE VALIDATION NOZZLE

For the design it is considered the expansion of ideal air through a fully centripetal nozzle, meaning that the relative velocity $\bar{w}$ only has a radial component, as in Fig. (3.1a). The boundary conditions that the flow should fulfill are:

- Inlet: Total conditions ($T_{tot,in}$, $P_{tot,in}$), static pressure (p_{in}) and relative flow velocity (w_{in}).
- Outlet: static pressure (p_{out}).

The frame of the nozzle is built by selecting the inlet and outlet cross sectional area A_{in} and A_{out} and a throat area A_{th}. The inlet area is determined by mass conservation as

$$A_{in} = \frac{m}{\rho_{in} w_{in}}, \tag{3.25}$$

where the inlet tensity and relative velocity, ρ_{in} and w_{in} are calculated as

$$u_{in} = \omega R_{in}, \tag{3.26}$$

$$v_{in} = \sqrt{w_{in}^2 + u_{in}^2}, \tag{3.27}$$

$$h_{in} = \sqrt{2c_p T_{tot,in} - v_{in}^2}, \tag{3.28}$$

$$T_{in} = c_p h_{in}, \tag{3.29}$$

$$\rho_{in} = \frac{p_{in}}{R T_{in}}. \tag{3.30}$$

R with no subscript stands for the gas constant. The cross sectional area A_{out} is determined by means of mass, rothalpy and entropy conservation as:

$$A_{out} = \frac{m}{\rho_{out} w_{out}}. \tag{3.31}$$

through equations (3.32)-(3.37):

$$T_{out} = T_{in}\left(\frac{p_{out}}{p_{in}}\right)^{\frac{\gamma}{\gamma-1}}, \tag{3.32}$$

$$\rho_{out} = \rho_{out}\left(\frac{T_{out}}{T_{in}}\right)^{\frac{1}{\gamma-1}}, \tag{3.33}$$

$$h_{out} = \frac{\gamma}{\gamma-1}\frac{p_{out}}{\rho_{out}}, \tag{3.34}$$

$$I = h_{in} + \frac{1}{2}\left(w_{in}^2 - u_{in}^2\right), \tag{3.35}$$

$$u_{out} = \omega R_{out}, \tag{3.36}$$

$$w_{out} = \sqrt{2\left(I - h_{out}\right) + u_{out}^2}. \tag{3.37}$$

The throat area is determined by means on the sonic line: a throat location along the nozzle is arbitrarily chosen and at that location the area is imposed to intersect the sonic line. The throat location is specifically chosen to have $A_{th} > A_{in}$ to prove that the physical throat does not necessarily coincide with a geometrical one. The area distribution along the nozzle is finally determined by simple interpolation between the three points (inlet, throat and outlet). The resulting area distribution and its position with respect to the sonic line are represented in Fig. (3.4), while in Tab. (3.3) are reported the imposed boundary conditions and the resulting cross sectional area at inlet, throat and outlet.

Table 3.3: Boundary conditions and nozzle geometry

Inlet	$\dot{m}$	[kg/s]	0.037
	$T_{tot,in}$	[k]	580
	$p_{tot,in}$	[bar]	20.4
	p_{in}	[bar]	10.86
	w_{in}	[m/s]	420.44
	R_{in}	[m]	0.11
	A_{in}	[m^2]	$1.10\ 10^{-5}$
Outlet	p_{out}	[bar]	8
	R_{out}	[m]	0.1
	A_{out}	[m^2]	$1.11\ 10^{-5}$
Throat	R_{th}	[m]	0.88
	A_{th}	[m^2]	$1.15\ 10^{-5}$

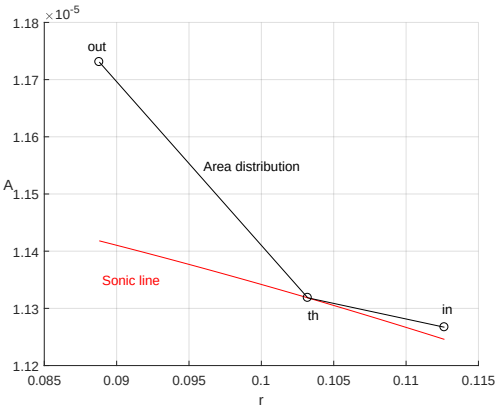

Table 3.4: Area distribution of nozzle used for validation

The obtained area distribution is used in the finite volume solver and the solutions of the flow are compared to the ones initially imposed to determine the nozzle geometry. An overview on the validation process is given on the scheme represented in Fig. (3.6), while the output of the comparison in between the results of finite volumesolver and the imposed boundary conditions is reported in Tab. (3.5). The percentage difference in between the FVS and the boundary conditions is defined as:

$$\%diff = \frac{|val_{FVS} - val_{BC}|}{val_{BC}}. \tag{3.38}$$

From results in Tab. (3.5) is evident that the maximum percentage difference achieved is of 0.13%. In particular, the fact that the difference on the mass flow is of 0.02% means that the location and cross sectional area of the throat where precisely determined and that the sonic line is a valuable design tool. This was proved for ideal conditions, while a further verification is needed for the real gas case.

Table 3.5: My caption

		% diff
$\dot{m}$	[kg/s]	0.02
w_{in}	[m/s]	0
p_{in}	[bar]	0.01
p_{out}	[bar]	0.13

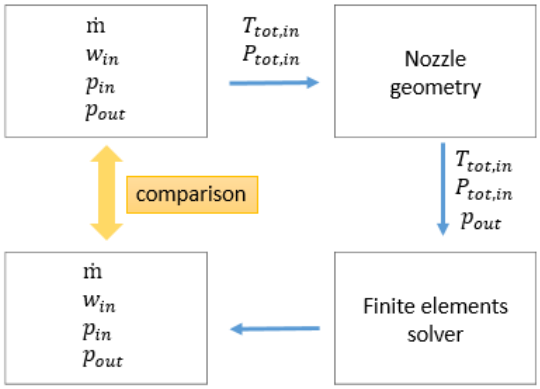

Table 3.6: Validation scheme

3.6.2. FLOW-AREA DIRECT RELATION

In Section 3.6.1 the outlet cross sectional area was specified in order to obtain a specific pressure at the outlet of the nozzle. However, this was possible thanks to the fact that one thermodynamic property (in the current case pressure) was imposed as a boundary condition. In the current section a different question is proposed: can the flow be fully specified along the nozzle, where no thermodynamic property is initially known? This is done by validating the analytic solution method proposed in Section 3.4, validation is carried out comparing ASM results to FVS results, a scheme is represented in Fig. (3.8).

In Fig. (3.11) are represented the flow solutions for velocity, relative Mach number and pressure for both methods; the percentage difference in between ASM and FVM is plotted as well. In particular, in Tab. (3.7) are reported the maximum, minimum and average difference, calculated as:

$$\%diff = \frac{|val_{FVS} - val_{ASM}|}{val_{FVS}}. \tag{3.39}$$

From Tab. (3.7) it is evident that the two methods provide comparable results. The maximum average deviation is of 0.11%, while the maximum difference between the two solvers occurs in proximity of the throat, as shown in Fig. (3.11). This is because ASM solver is very sensitive to the throat cross sectional area, which is determined numerically by means of the sonic line. A control was added to the solver in order to approximate small area deviations from the sonic line to a physical throat and overcome the discretization problem.

Table 3.7: Deviations in between the analytic solution method (ASM) and the finite differences solver (FVS)

		Solutions deviation %		
		ave	min	max
Velocity	w	0.09	0.00	0.09
Mach number	M	0.11	0.00	1.84
Pressure	p	0.11	0.00	2.22

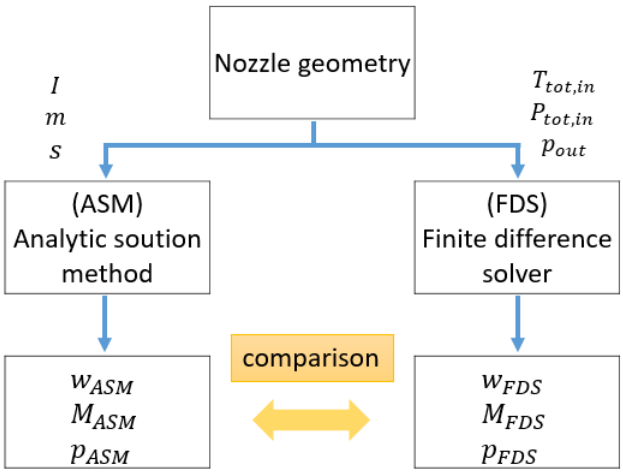

Table 3.8: Validation scheme

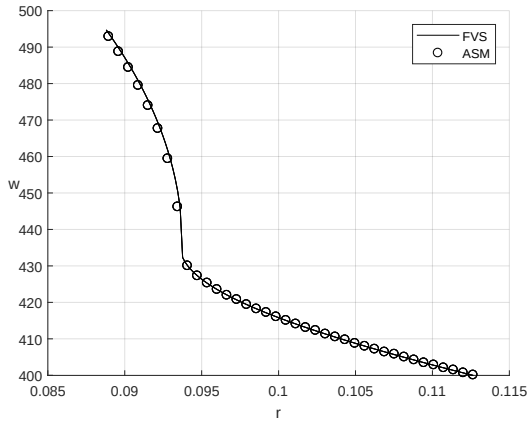

(a) Velocity in the rotating frame of reference

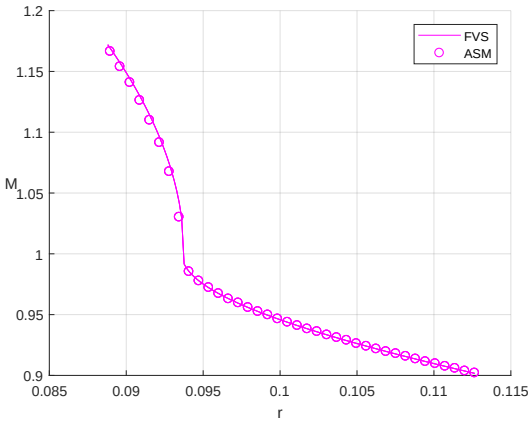

(b) Mach number

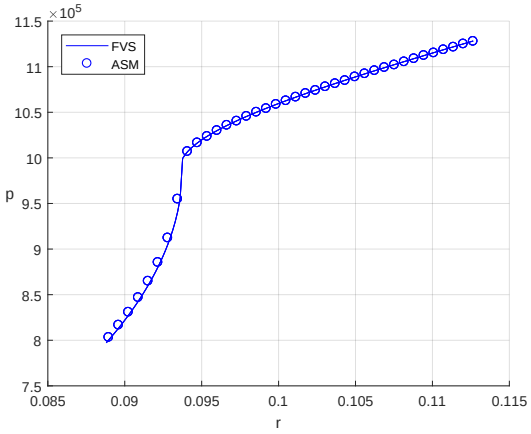

(c) Pressure

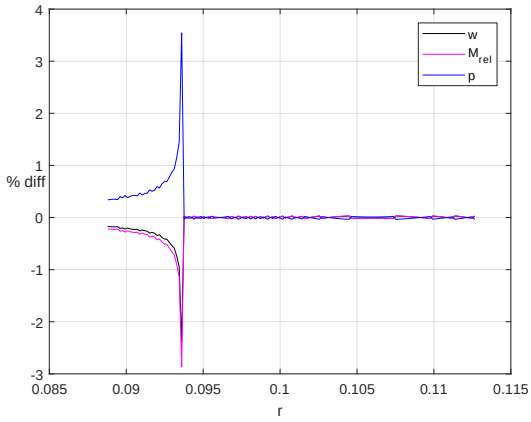

(d) Difference in between methods

Figure 3.11: Final blade design

It is concluded that the 1D analysis done in the current chapter provides a good understanding of the system and of the flow behaviour: a sonic line is identified and the physical constrains to an isentropic expansion are determined. For an ideal gas the sonic line is a valuable tool to predict the throat position and it cross sectional area. For precise input values of I, $\dot{m}$ and s, the analytic method and the finite volume method are comparable, meaning that AMS can be used for inverse nozzle design.

4

BLADE DESIGN

In the current chapter the design methodology for turbine rotor blades is presented. As previously explained, the system is approached as a 1D flow through a nozzle in rotation, therefore the blades are shaped in order to obtain an imposed nozzle. The design proposed follows an approach between the direct and the inverse one: an initial shape is initially generated by means of a parametrization developed in this chapter. Afterwards, it is verified if the area distribution obtained along the nozzle allows for an isentropic expansion and if a physical throat is provided. This is done by checking if there are intersections in between the area distribution and the sonic line on the (r, A) plane, Section 3.3. If a throat is not provided, the blade shape is modified to change the area distribution. The advantage of this method over a fully direct one is that the flow properties are not calculated at each iteration and the target (having one single intersection in between the area distribution and the sonic line) is well defined.

The design is carried out in two stages, a preliminary design and a detailed design. The first one sets the main architecture of the blade, ensuring that boundary conditions and geometry constrains are respected. The second ones focuses on the detailed shape of the blade, obtained through a blade parametrization and iteration.

4.1. PRELIMINARY DESIGN

During the preliminary design, the focus is set on the channel in between the blades, while the shape of the blades is not considered. The inlet/outlet cross sectional area and the flow direction are chosen in order to fulfill the boundary conditions. In fact, it must be taken into account that the rotor is not an independent element: flow conditions are imposed upstream by the stator and downstream by the condenser. If the design of the rotor does not match with the other elements, the flow necessarily has to adapt to the external conditions, leading to consistent entropy losses. In the current section all the system boundary conditions are briefly discussed, the inlet and outlet flow direction and cross sectional area calculated my means of a one-dimensional analysis.

4.1.1. BOUNDARY CONDITIONS AND CONSTRAINS

Before discussing the boundary conditions, it is worth recalling the numbering used for stator and rotor: 1) stator inlet, 2) stator outlet/rotor inlet, 3) rotor outlet. A distinction is made in between constrains imposed by the system and the ones imposed by the designer. The first ones depend either on the upstream and downstream conditions or on the main dimensions imposed on the turbine; they are assumed to be fixed and therefore they cannot be changed during the design process. The second ones, instead, can be changed in order to adapt the rotor's working conditions to the required ones. All the constrains and boundary conditions relevant for the design are listed in Tab. (4.1).

To the first category belong the total conditions $T_{tot,2}$ and $P_{tot,2}$ at the inlet of the rotor, which are determined by the flow conditions at the outlet of the stator. The stator also sets the mass flow (due to chocked conditions) and the flow direction α_2 at the rotor inlet. At the rotor outlet the static pressure p_3 is imposed by

Table 4.1: Blade design boundary conditions and constrains

	Parameter	Symbol
Operating conditions	Shaft speed	ω
	Mass flow	$\dot{m}$
	Total temperature	$T_{tot,2}$
	Total pressure	$P_{tot,2}$
	Rotor inlet pressure	p_2
	Rotor outlet pressure	p_3
Geometry	Rotor inlet radius	R_2
	Rotor outlet radius	R_3
	Number of blades	N_b
Flow direction	Inlet flow angle	α_2
	Outlet flow angle	α_3

the condenser. Finally, the number of blades N_b, the stator inlet radius R_1 and the rotor outlet radius R_3 are assumed to be imposed as well.

During the design process it is possible to choose the shaft speed ω and to impose the rotor inlet static pressure p_2 and radius R_2. The blade angle α_3 at the outlet of the rotor needs to be determined as well. These choices affect the degree of reaction, the relative Mach number at the inlet of the rotor and the total work extraction; the possibility of choosing these parameters allows for more freedom in the design, so that optimal working conditions can be achieved. The shaft speed, rotor inlet pressure, the inlet radius and the flow direction are crucial in order to determine velocity triangles and the cross sectional area, so they must be set as well during the preliminary design. The choice procedure of these parameters, however, cannot be strictly determined since it strongly depends on the conditions that the designer wants to achieve in the rotor. The current chapter aims to give a general design method, therefore ω, p_2, R_2 and α_3 are treated as flexible parameters that need to be determined in a previous analysis.

4.1.2. ONE-DIMENSIONAL ANALYSIS

The preliminary design determines the main frame of the blade, ensuring that the inlet and outlet boundary conditions are respected: the flow enters the rotor with an absolute velocity $\bar{v}_2$ and at should exit with an absolute velocity $\bar{v}_3$. However, the whole system is analyzed in the relative frame of reference, so the velocity component $\bar{w}$ must be derived at the inlet and outlet of the nozzle (Location 2 and Location 3). This is done by means of the velocity triangles, introduced in Section 2.1. Velocity is analyzed in terms of its components (v, w and u) and of flow direction (α and β); the flow is assumed to have no velocity component in the z direction, as represented in Fig. (4.1). All conditions at Location 2 and Location 3 are determined through the system of equations (4.1):

$$\begin{cases} I = h + \frac{1}{2}\left(w^2 - u^2\right) = const \\ s = const \end{cases} \tag{4.1}$$

The expansion is assumed to be isentropic, where the entropy s is calculated according to the total conditions and the turbine inlet. Because of the non-ideal behaviour of toluene, all properties along the flow are calculated with ®RefProp through Eq. (4.2-4.6):

$$s = s(T_{tot}, p_{tot}), \tag{4.2}$$

$$T = T(p, s), \tag{4.3}$$

$$\rho = \rho(p, s), \tag{4.4}$$

$$h = h(p, s), \tag{4.5}$$

$$c = c(p, s). \tag{4.6}$$

Velocity triangles are finally evaluated through the general system (4.7)

$$\begin{cases} w_\theta + u = v_\theta \\ w_r = v_r \end{cases} = \begin{cases} wsin\left(\beta\right) + u = vsin\left(\alpha\right) \\ wcos\left(\beta\right) = vcos\left(\alpha\right) \end{cases} \tag{4.7}$$

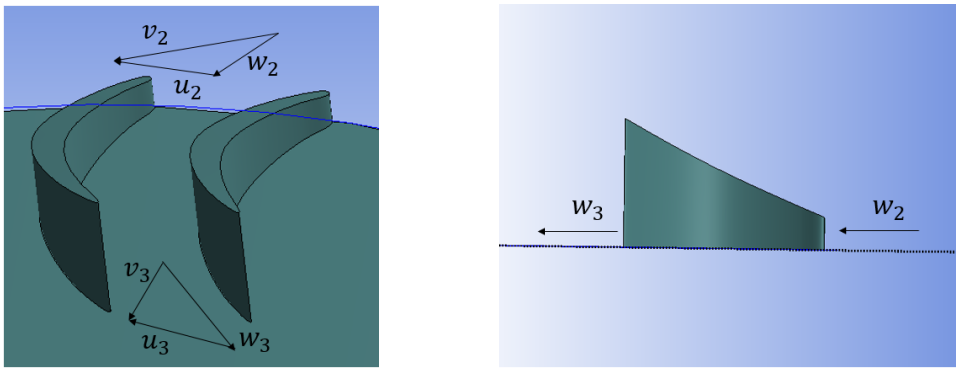

(a) Velocity triangles from blade orthogonal view (b) Velocity triangles from a blade lateral view

Figure 4.1: General overview of velocity triangles at the inlet and outlet of the rotor

which considers each velocity component in the frame of reference (r,θ) introduced in Section 2.2. The velocity $\bar{u}$ has only one component in direction θ and is always defined as

$$u = \omega R. \tag{4.8}$$

Angles and velocity components are represented in Fig. (4.2).

(a) Components in the absolute and relative frame of reference (b) Components of one vector in the the frame of reference (r,θ)

Figure 4.2: Example of general velocity triangle and of its components

Once the velocity components and the thermodynamic properties are determined, the flow absolute and relative Mach number can be calculated as:

$$M = \frac{v}{c}, \tag{4.9}$$

$$M_{rel} = \frac{w}{c}, \tag{4.10}$$

Velocity triangle 2: Stator outlet/Rotor inlet The conditions at the outlet of the stator depend on the pressure p_2. Once this is set, the enthalpy h_2 is determined as $h_2 = h(p_2, s)$ and the speed v_2 is calculated by means of Eq. (4.11). The flow angle α_2 is known because imposed by the stator, the peripheral velocity it is calculated as in Eq. (**??**):

$$v_2 = \sqrt{2\left(H_{tot,2} - h_2\right)}. \tag{4.11}$$

Since the speed of two velocity components and one angle (v_2 u_2 and α_2) are known, as schematized in Fig. (4.3), system (4.7) can be solved and also the speed w_2 and the angle β_2 are determined. The Mach number, both in the absolute and relative frame of reference, is calculated by means of Eq. (4.9) and (4.10). The speed of sound, as all the other thermodynamic properties, are obtained through the set of equations of state.

(a) Location 2 (b) Location 3

Figure 4.3: Velocity triangle components initially known through the boundary conditions

Velocity triangle 3: Rotor outlet Since the pressure p_3 is set, the thermodynamic properties at the outlet of the rotor can again be easily calculated by means of (4.2)-(4.6) by setting $p = p_3$. In the rotor the quantity conserved along the expansion is the rothalpy I, which is therefore used for the calculation of the outlet velocity w_3:

$$I = h_2 + \frac{1}{2}\left(w_2^2 - u_2^2\right), \tag{4.12}$$

$$u_3 = \omega R_3 \tag{4.13}$$

$$w_3 = \sqrt{2\left(I - h_3\right) + u_3}. \tag{4.14}$$

Again, two velocity components (w_3, u_3) and one angle (α_3) are known, as shown in Fig. (4.3b). The velocity triangle at Location 3 is therefore fully determined and the relative and absolute Mach number can be calculated again through Eq. (4.9)-(4.10).

Cross sectional area The design of the right cross sectional area in the nozzle is crucial in order to fulfill mass conservation and the pressure boundary conditions. Since the design is carried out for the rotating frame of reference, it is underlined that in the current thesis work the cross sectional area is defined with respect to the velocity component $\bar{w}$, as shown in Fig. (4.4).

At the rotor inlet and outlet the velocities are already imposed by the velocity triangles, while all thermodynamic properties are imposed by the isentropic relations (4.2)-(4.6). Therefore, the cross sectional area is calculated by means of mass conservation as:

$$A = \frac{\dot{m}}{\rho w}, \tag{4.15}$$

where Eq. (4.15) is directly derived from mass conservation $\dot{m} = \rho A w$.

The cross sectional area A determined in the preliminary design is a first approximation, meant to give the order of magnitude of the cross sectional area required at the inlet and outlet of the rotor. However, A_2 and A_3 depend on the radial position of the nozzle inlet and outlet point, which will be discussed with the detailed design. Therefore, in Section 4.2 a correction of the cross sectional area will be provided.

During the nozzle preliminary design, usually also the throat area is determined, which imposes choked conditions. However in section (3.3) it was seen that in a rotating nozzle the throat area depends on the radius. However, in this case the shape of the blades is not taken into account yet, therefore no criteria is defined in order to choose the throat location. Choked conditions are therefore discussed during the detailed blade design.

4.2. DETAILED BLADE DESIGN

Through the detailed design the final blade shape is achieved. As mentioned in Section 1.1.2, one of the main drawbacks of inverse design approaches is that imposing the flow properties along the nozzle leads to unphysical blade dimensions. This problem was avoided by imposing a blade parametrization, meant to satisfy some main blade requirements:

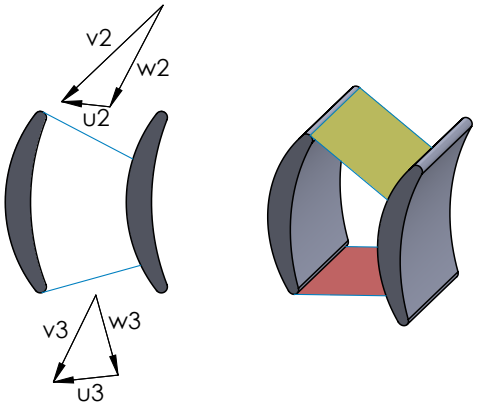

Figure 4.4: Cross section definition

- the blade camber line should not have any change in concavity,
- the blade has to have physical dimensions. The thickness distribution along the camber line has to be such to handle the forces acting on the blade,
- the blade height has to either be constant or monotonically increasing moving from the outer radius to the inner one.

The blade geometry is built around the camber line, which is determined in the first step of the detailed blade design. The overall shape is controlled through parameters as the stagger angle and the blade thickness. These parameters are overall 14, listed in Tab. (4.2), and represent all the of freedom allowed by the design methodology described. Their meaning and influence will be explained along with the methodology.

Table 4.2: Degrees of freedom of the blade parametrization

Degrees of freedom	**Symbol**
Stagger angle	δ
Three locations along the camber line	loc_A, loc_B, loc_C
Blade thickness at each location	th_A, th_B, th_C
Blade slope at 2 locations	slope_A, slope_C
Blade curvatures at LE and TE	fac_{LE}, fac_A fac_{TE}, fac_C
Control point for blade height	R_{P2}

The detailed design is based on shaping separately the blade section, on the plane (x, y), and the blade height, on the plane (r, z). The different planes are recalled in Fig. (4.5). The blade section parametrization is provided in order to control the shape and the thickness, while the function describing the blade height is determined in order to avoid negative slopes. A mid line Ψ in between two blades is drawn and the flow is assumed to follow that path, therefore Ψ is treated as a streamline. The area distribution is calculated at each point along Ψ. The shape of the blades is finally changed iteratively till reaching a proper area distribution along the stream line; the whole procedure scheme is described in Scheme (4.6) and will be explained into detail in the current section.

4.2.1. CAMBER LINE

The camber line is the mean line in between the pressure and the suction side of the blade and it determines the main flow direction during the expansion. In the current case the main flow direction at the inlet and outlet of the rotor was determined in the preliminary design, therefore the camber line should be designed in order to guarantee the expected flow. As previously stated, no changes of concavity should occur in the span

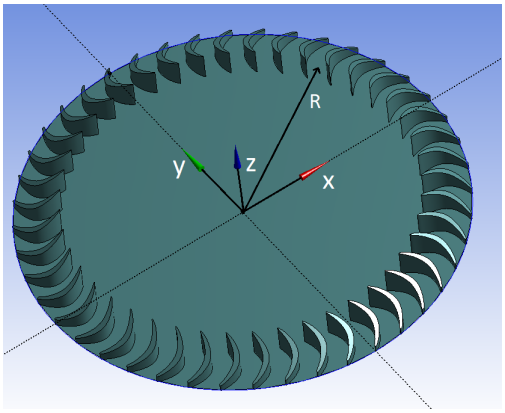

Figure 4.5: Frames of reference (x, y) and (r, z) in the rotor

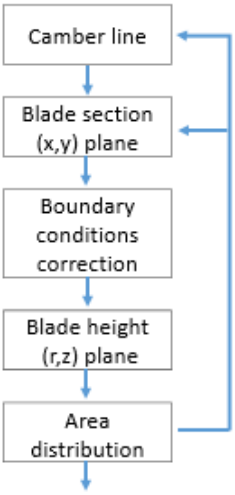

Figure 4.6: Work scheme wor the detailed blade shaping

wise direction and the geometry should be as smooth as possible. In order to satisfy these requirements, it was chosen a parametrization by means of a Bezier curve of second order, described by Eq. (4.16):

$$P(t) = (1-t^2)P_1 + 2t(1-t)P_2 + t^2P_3,\ t \in [0,1] \tag{4.16}$$

Through Eq. 4.16 it is possible to specify three points in a plane, P_1, P_2 and P_3 and to draw a curve connecting P_1 and P_3. The shape and concavity of the curve are determined by the position of point P_2; in P_1 and P_3 the curve is always tangent to the line connecting respectively $P_1 - P_2$ and $P_2 - P_3$. In Fig. (4.16) it is evident that by moving P_2 form location a to location b the curve substantially changes shape.

The camber line is therefore built by means of a Eq. (4.16), where P_1 and P_3 are respectively the leading and trailing edge of the blade. The construction is done on the (x, y) plane for one single blade, the leading and trailing edge are constrained to lay respectively at a distance R_2 and R_3 from the center of rotation. Their relative position however is not constrained by the system and it is specified by mean of the stagger angle δ. Therefore, the location of P_1 and P_3 is set as in Eq. (4.29):

$$\begin{aligned} P_1 &= (0, R_2) \\ P_3 &= (-R_3 sin\delta, R_3 cos\delta) \end{aligned} \tag{4.17}$$

Point P_2 is set at the intersection in between two lines passing through P_1 and P_3 and having an angle respectively of β_2 and β_3 with respect to the radial position, as shown in Fig. (4.7b).

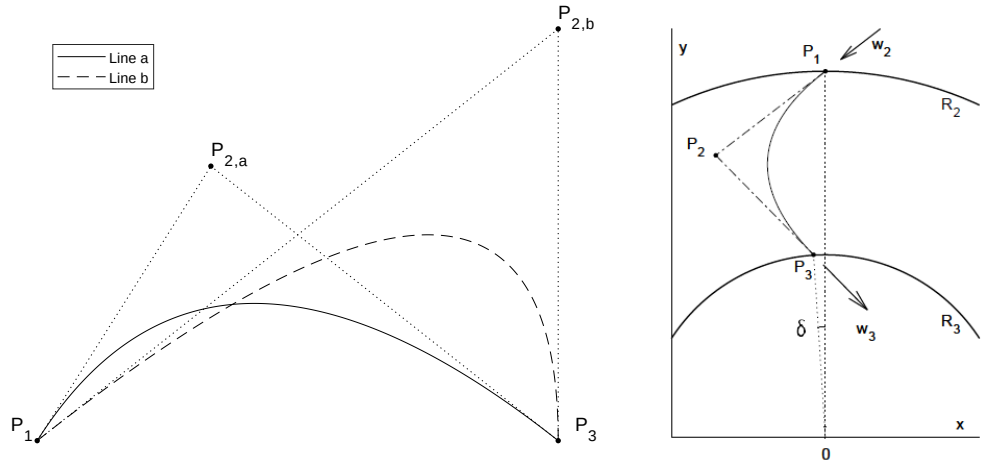

(a) Influence of the postion of P_2 on the space of a Bezier curve

(b) Construction of the camber line by means of a Bezier curve

Figure 4.7

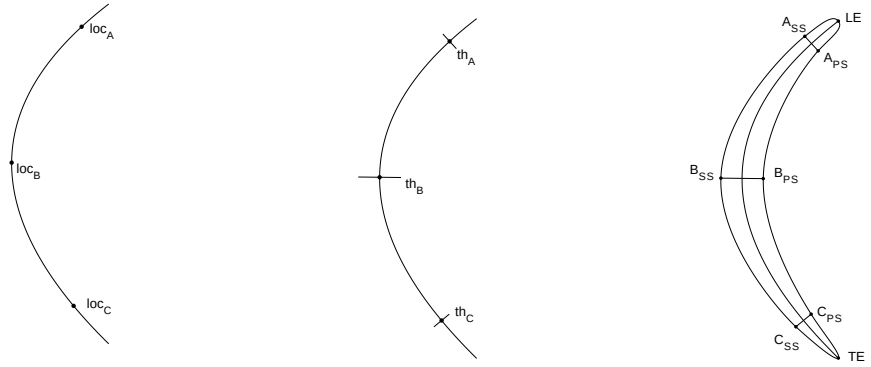

(a) Control points along the camber line

(b) Blade thickness parametrization

(c) Blade construction

Figure 4.8: Main steps for building the blade section

4.2.2. BLADE SECTION AND CROSS SECTIONAL DISTANCE

The blade section is built on the plane (x, y) by using the camber line as a main frame and imposing a symmetric blade thickness around it. Initially three points are selected along the camber line, A and C in proximity respectively of the leading and trailing edge, B positioned in the central area of the camber line, Fig. (4.8a). A blade thickness is assigned to each point in the direction tangential to the camber line, Fig. (4.8b); the thickness th_B is always specified as grater than the other ones, meaning that location B is the one of maximum thickness along the blade. Finally the blade section is created by spines connecting points $LE-A_i$, $A_i-B_i-C_i$ and C_i-TE, where i stands either for SS (Suction Side) or PS (Pressure Side), Fig.(4.8c). Different splines are used to implement the leading/trailing edge and the main body, which are therefore discussed separately.

Leading/Trailing edge The leading and trailing edge are built following the same procedure, therefore only the leading edge is explained as an example. Two splines are built, connecting respectively $LE-A_{SS}$ and $LE-A_{PS}$. Splines are drawn by means of a ®Matlab built in function, which is here describe only in terms of its inputs:

$$\text{spline} = \text{spline}(slope_1, fac_1, points, slope_2, fac_2) \tag{4.18}$$

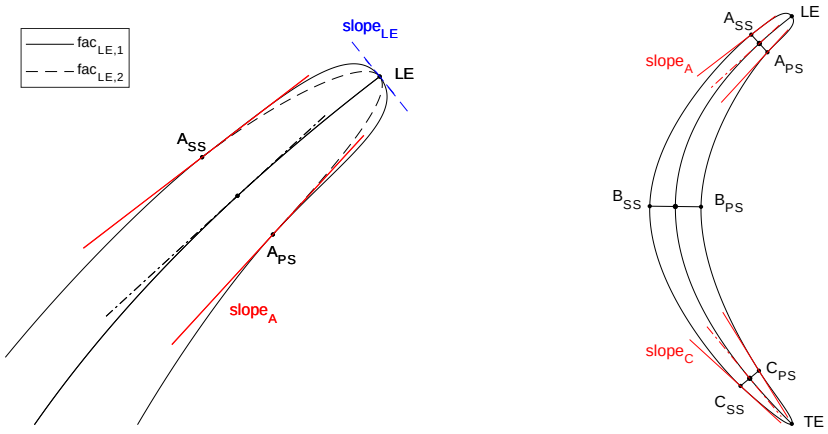

(a) (b)

Figure 4.9: Leading and trailing edge construction

The terms $slope_1$ and $slope_2$ allow to specify the slope that the curve should have at the first and last point, while fac_1 and fac_2 determine the curvature again at the first and last point. The term $points$ includes the coordinates of all points to be connected.

Therefore the splines at the leading is created as:

$$\text{spline} = \text{spline}(slope_{LE}, fac_{LE}, points, slope_A, fac_A)$$

The lines obtained are represented in Fig. (4.9). The slope at the leading edge (blue line in Fig. (4.9)) is perpendicular to the camber line, while the lines tangent to the spline at A_{PS} and A_{SS} (red lines in Fig. (4.9)) are symmetric with respect to the camber line. The slope at the leading edge depends only on the inlet velocity triangle, while the designer has to specify $slope_A$. The factor determining the curvature is not physically visible in figure, however two different blade shapes are represented for $fac_{LE,1}$ and $fac_{LE,2}$, being $fac_{LE,1} > fac_{LE,2}$. It is evident that for higher factors, the radius of curvature of the spline increases.

What stated for the leading edge stands also for the trailing edge, with the only difference that $slope_{TE}$ depends both on the outlet velocity triangle and on the stagger angle.

Blade main body For the main body along the blade are used two splines, one connecting the suction side points (A_{SS}, B_{SS}, and C_{SS}) and one connecting the pressure side points (A_{PS}, B_{PS}, and C_{PS}), represented in Fig. (4.8c). The blade should be as smooth as possible and it is preferable not to have any sudden change of slope along it. This might occur at the juncture points in between different splines, so at points A_i and B_i. At these locations, slope continuity is guaranteed by specifying the mid splines as in Eq. (4.18) and imposing the same slope as in the leading and trailing edge, therefore $slope_{LE}$ and $slope_{TE}$. Compared to the leading and trailing edge, an additional degree of freedom is added due to fact that the line passes through three points instead than two. By always specifying $th_B > th_{A/C}$ it is guaranteed that in between points A and B no changes in concavity occur.

Once the section of the blade is fully determined, a second blade is drawn by rotating the first of an angle $ang = 360/N_b$, depending on the total number of blades in the rotor. Another line is drawn by rotating the camber line of $ang/2$, as shown in Fig. (4.10a), representing the mid line of the nozzle. The first point of the stream line, Ψ_{in}, is therefore determined as the intersection in between the mid line and the line perpendicular to it passing through the leading edge of Blade$_1$, Fig. (4.10a). The streamline outlet, Ψ_{out}, is determined at the same way with respect to the trailing edge of Blade$_1$. The stream line Ψ is used to evaluated the cross sectional area at each point along the nozzle; however, defining Ψ as a streamline is a strong assumption and does not represent the real flow in between the blades. The real flow behaviour is too complicated to be set a

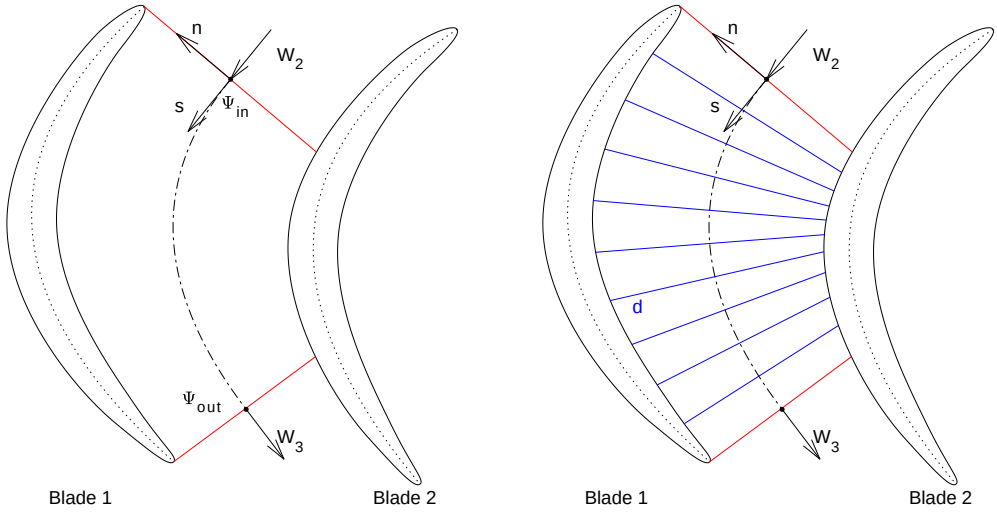

(a) Blade passage and mid line

(b) Distance in between blades along the mid line

Figure 4.10: Blade passage, mid line and distance in between blades

priori and it would not be convenient for the design methodology.

Finally, for each location along the streamline, the cross sectional distance d is evaluated assuming that the flow relative velocity is always tangent to Ψ, therefore having only a component s in the frame of reference (s, n), Fig. (4.10b). The distance distribution d is initially determined along the mid line as $d = d(s)$ and afterwards converted to polar coordinates in order to redefine it as $d = d(r)$.

4.2.3. OUTLET CROSS SECTIONAL AREA CORRECTION

During the preliminary design the inlet and outlet cross sectional area were calculated. The rothalpy I was determined at the inlet of the rotor and it was afterwards used to calculate the velocity w_3 at the outlet. Finally, the cross sectional area was computed by means of Eq. (4.15).

Equations (4.11)-(4.15) were evaluated at R_2 and R_3 in order to determine the velocity triangles. The design however aims to build a nozzle around a the mid line Ψ, so for a consistent design the boundary conditions have to be specified at Ψ_{in} and Ψ_{out}. By looking at Fig. (4.10a) it is obvious that the points Ψ_{in} and Ψ_{out} are located at different radii than R_2 and R_3. The inlet velocity v_2 is determined by the stator, while w_2 depends,in on the peripheral velocity by means of $\bar{w} = \bar{v} - \bar{u}$; since $u(R_2) < u(R_{\Psi,in})$, $w(R_2) \neq w(R_{\Psi,in})$. Therefore the inlet and outlet cross sectional area are corrected through the set of equations (4.19)-(4.25):

$$u_2^* = \omega R_{\Psi,in}, \tag{4.19}$$

$$w_2^* = w(v_2, u_2^*), \tag{4.20}$$

$$I^* = h_2 + \frac{1}{2}\left(w_2^{*2} - u_2^{*2},\right) \tag{4.21}$$

$$u_3^* = \omega R_{\Psi,out}, \tag{4.22}$$

$$w_3^* = \sqrt{2\,(I^* - h_3) + u_3^*}, \tag{4.23}$$

$$A_2^* = \frac{\dot{m}}{\rho_3 w_2^*}, \tag{4.24}$$

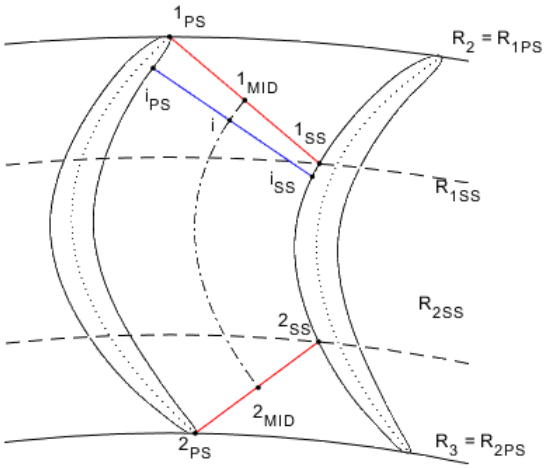

Figure 4.11: Blade numbering, (x, y) plane

$$A_3^* = \frac{\dot{m}}{\rho_3 w_3^*}, \tag{4.25}$$

where w_2^* in Eq. (4.20) is calculated by means of system (4.7).

The deviation in between the values calculated in the preliminary design and the corrected ones strongly depends on the geometry, an error range was not calculated. However, for the particular test case that will be discussed in Chapter **??**, it was seen that an area deviation of around 5% is achieved for a rothalpy deviation of 1%. The correction leads to a mismatch in between the inlet blade angle and the flow angle β_2, leading to an incidence angle. However, the inlet and outlet area are the ones that guarantee that boundary conditions are respected, so the priority was given to reducing the area error as much as possible.

4.2.4. BLADE HEIGHT

The blade height distribution h_b plays an important role in determining the cross sectional area, therefore the parametrization of $h_b(r)$ has to take into account that A_2^* and A_3^* need to be obtained at the inlet and outlet of the nozzle. To do so, it is first important to discuss how is the cross sectional area calculated; the explanation makes use of the numbering introduced in Fig. (4.11)-(4.12). As an example it is discussed the cross sectional area at the inlet, Fig. (4.12), however the explanation stands for all points along the nozzle. Two blades with a linear height distribution are taken into account, the blade thickness is assumed to be constant moving from the hub to the tip. The cross sectional area is analyzed in the plane (n, z) at a fixed coordinate s. It is evident that the blade height is not constant along the n and can be defined as $h_b = h_b(n)$. In Fig. (4.12), A_2 is the polygon formed by points $1_{SS,T}$, $1_{SS,H}$, $1_{PS,T}$ and $1_{PS,H}$, where the subscript H stands for hub and T for tip. If the blades had a non-linear height distribution, the line connecting $1_{SS,T}$ - $1_{PS,H}$ would be curved, therefore the area of the polygon has to be calculated by means of an integral:

$$A = \int h_b(n)\, dn. \tag{4.26}$$

Due to the fact that at each location along s the blade $h_b(n)$ is not constant, the blade height has to be expressed as a function of the radius and redefined as $h_b = h_b(r)$. This implies that it a blade height distribution is imposed to provide a certain cross sectional area in one location, the cross sectional area of other points along Ψ is affected. To better explain the concept, location i in Fig. (4.11) is taken into account: the area at location i depends on the cross sectional distance d_i and on the the blade height distribution in between points i_{PS} and i_{SS}. Assuming that the blade cross section was already fixed according to Section (4.2.2), d_i is already imposed and cannot be changed. In addition, if the blade height is defined in order to have a certain inlet area, also the blade height distribution in between points 1_{PS} and 1_{SS} is imposed. Therefore to obtain a

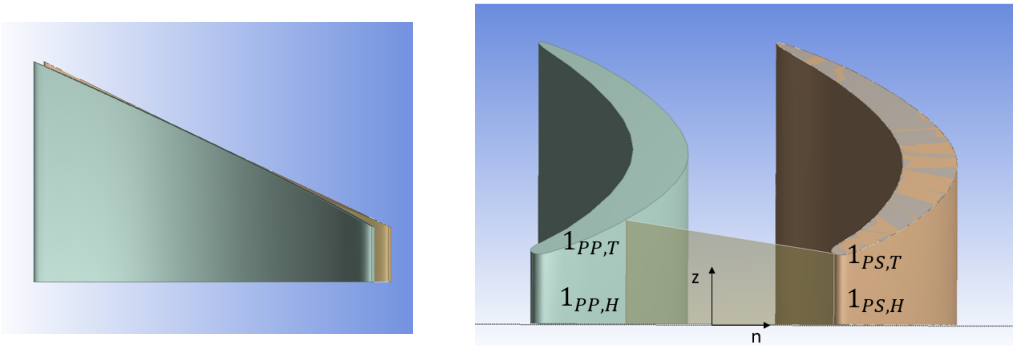

Figure 4.12: Blade numbering, (n, z) plane

certain area A_i only the height distribution in between 1_{SS} and i_{SS} can be changed, which in most cases leads to a non physical blade shape. Because of this, it was chosen provide a blade height parametrization such that:

- the area distribution along the nozzle is an output;
- the corrected inlet and outlet cross sectional areas A_2^* and A_3^* are respected,
- the blade height monotonically increases moving from R_2 towards R_3,
- no abrupt discontinuities of slope or concavity occur along the blade.

This is achieved by splitting the blade height distribution in two different sections, R_{1PS} - R_{1SS} and R_{1SS} - R_{2PS}.

Section $R_{1PS} - R_{1SS}$: the first part of the blade height distribution aims to build a proper inlet cross sectional area. In this section, a constant blade height is imposed. The choice is due to two main factors:

- imposing a constant height allows for a well defined slope, which is easier to reproduce also at the juncture point with the second section of the height distribution;
- depending on the inlet pressure p_2, the required inlet cross sectional area can significantly change. A constant area distribution is the one that allows for a maximum inlet blade height, while if the height h_{1SS} increases, the area difference necessarily has to be compensated by a lower h_{1PS}. If the inlet height is too small, problems related to viscosity and boundary layers may occur, therefore imposing a constant height distribution in between points R_{1PS} and R_{1SS} limits the risk of reaching non-physical blade height.

For a constant blade height, $h_{1PS} = h_{1SS} = h_{in}$, therefore Eq. (4.26) can be written as (4.27) and the inlet blade height is calculated as in Eq. (4.28):

$$A = d \cdot h_b, \tag{4.27}$$

$$h_{b,in} = \frac{A_2^*}{d_{in}}. \tag{4.28}$$

Section $R_{1SS} - R_{2PS}$: the second section of the height distribution has to guarantee at the same time slope continuity at point 1_{SS} and that the outlet cross sectional area is respected. This is done by means of an iterative process and defining the height distribution through a Bezier curve of 2^{nd} order, Fig. (**??**). Three control points P_1, P_2 and P_3 are needed: P_1 is set at the junction point in between the two sections and P_2 is set at the same height as P_1 with a smaller radius. This ensures that the Bezier curve at location P_1 has zero slope, as the first section of the height distribution. The point P_3 is set at radius R_{2PS} and its height h_3 is changed iteratively till the outlet boundary conditions are met. Therefore the three points have coordinates:

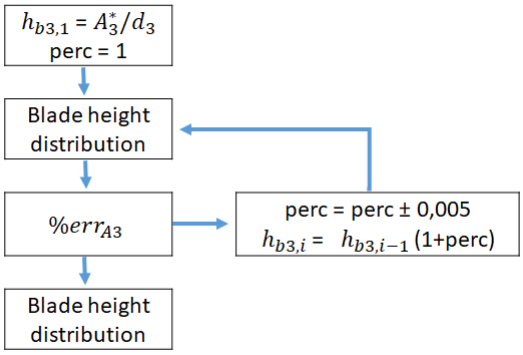

(a) Iteration scheme used to determine the blade height from point 1_{SS} to 2_{PS}

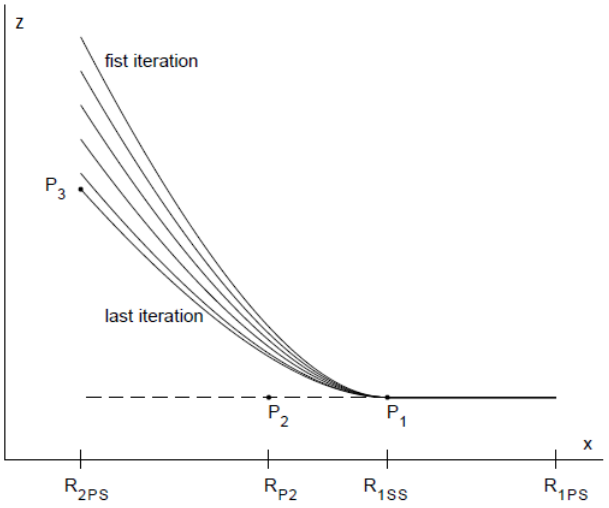

(b) Blade height $h_{b3} = h(r)$ at each iteration i

$$\begin{aligned} P_1 &= (R_{1SS}, h_{1SS}) \\ P_2 &= (R_{P2}, h_{1SS}) \\ P_3 &= (R_{2PS}, h_{3,i}) \end{aligned} \tag{4.29}$$

Where $h_{3,i}$ is the height of P_3 at each iteration. Iterations are carried out by following scheme (4.13a), an example is shown in Fig. (4.13b); the iteration scheme reads as follows:

- An initial guess for the height $h_{b,3}$ is calculated as: $h_{b,3} = A_3^*/d_3$. Therefore $P_3 = (R_{2PS}, h_{b,3})$
- A blade height distribution is calculated as a Bezeir curve through P_1, P_2 and P_3. This defines the cross sectional area on each point along Ψ
- The resulting outlet area A_{out} is calculated by means of Eq. (4.26). The error err with respect to A_3^* is calculated, if $abs(err) \leq err_{min}$ the blade height distribution is an output. If $abs(err) > err_{min}$ the height $h_{b,3}$ is changed and a new iteration starts.

4.2.5. AREA DISTRIBUTION

Once both the cross sectional distance in between blades and the blade height are imposed, the cross sectional area is defined at each point along the mid line Ψ. Therefore, both the geometry and the peripheral velocities are fixed and the nozzle can be analyzed according to the considerations done in Chapter 3 on a rotating nozzle.

The sonic line is calculated for the rothalpy I^* according to Chapter 3. The area distribution and the sonic line are plotted together and the relative position in between the two is taken into account. At the first attempts the area distributions provides either subsonic on non isentropic solutions, as in Fig. (4.14a). To obtain a transonic blade, it is fundamental that the area distribution touches the sonic line in at least one point, meaning that a physical throat is present. Ideally, the area distribution should decrease/increase smoothly to avoid recompressions of the flow along the nozzle. If these two requirements are not met, the design parameters are changed and the whole routine explained in Fig. (4.6) is repeated till an area distribution as in Fig. (4.14b) is obtained. No automatic iteration was implemented, therefore the design has to be changed manually depending on the area distribution obtained.

To conclude, in the chapter it was provided a methodology for the blade design. This consists of two parts: a preliminary design and a detailed design. The first one provides the main architecture of the blade and it is used as a starting point for determining the blade shape. The blade parametrization is done by means of 14

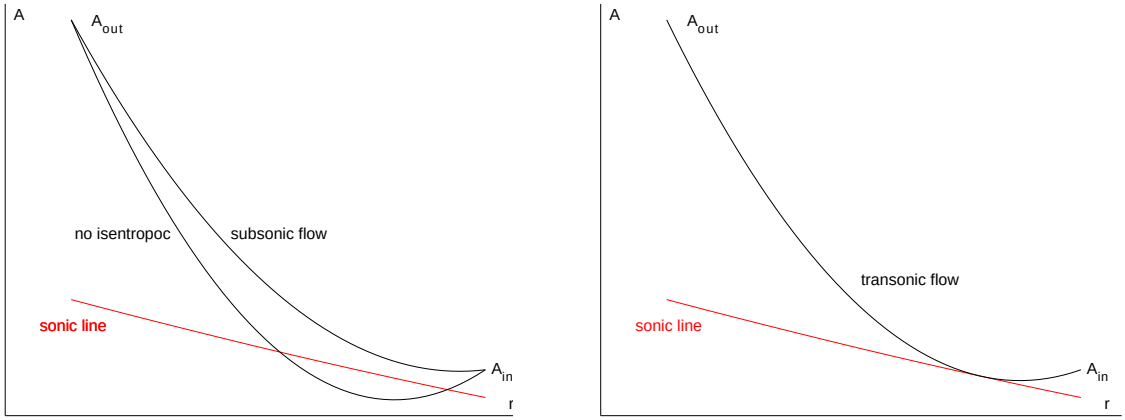

(a) Intermediate steps

(b) Target area distribution

Figure 4.14: Relative position between sonic line and area distribution at each blade iteration

variables, listed in Tab. (4.2), and it ensures that the blade has physical dimensions and a nozzle is created in between the blade channel.

5

APPLICATION TO TRIOGEN CASE

In the present chapter, the blade design methodology presented in Chapater 4 is applied to redesign Triogen's [6] turbine rotor. First it is given general information about the original rotor and previous analysis done on it. In the second section the blade parametrization is applied to obtain a blade shape. Finally, the obtained design is discussed under two different aspects: the capability of the blade parametrization to actually achieve the required design and the applicability of the proposed method for blade design. The resulting blade is simulated using CFD.

5.0.1. TRIOGEN TURBINE

Triogen turbine is chosen as a case study due to the optimization process it is going through. The original turbine design was already analyzed by means of CFD simulation by Harinck et Al. [1] in 2012 and different improvements were proposed, as explained in Chapter 1. In particular, with respect to the rotor the following changes were suggested:

- the rotor should run at higher speed of rotation,
- the leading and trailing edge blade angles should be increased,
- the blade curvature should decrease,
- the blade thickness should be increased.

The first suggestion is meant to reduce the flow relative Mach number at the rotor inlet, while the others are due to flow separation that was noticed in the CFD simulations, as introduced in Section 1.2. In Fig. (5.1) are highlighted the blade separation, occurring on the blade suction side, and a possible blade redesign suggested by Harinck et Al. [1]. The aspect ratio if the blade in figure was changed.

Since then, several optimized versions of the stator where introduced, which led to a different mass flow through the turbine [19]. The operating conditions have changed as well, as shown by the wide range of input conditions reported in Tab. (5.1); geometrical parameters were not reported due to confidentiality. All these changes were not followed by a rotor optimization. A more recent analysis on the original rotor, running at different conditions compared to the ones simulated by Harinck et Al. [1], was carried out by G. Otero [19]. The analysis was done once again by means of CFD. If Fig. (5.2a) are shown in red the regions where the relative flow speed is subsonic, in blue where it is supersonic; the aspect ratio of the figure was changed. It is noticed that transonic conditions are reached along the blade, however, in proximity of the exit (left side in the figure) the flow returns to subsonic conditions due to a strong shock wave. The presence of the shock was related to a hump in the area distribution along the nozzle mid line, Fig. (5.2b).

Therefore, it was concluded that a new rotor is needed, designed for the right mass flow and having blade angles and an area distribution along the nozzle fit for the current speed of rotation.

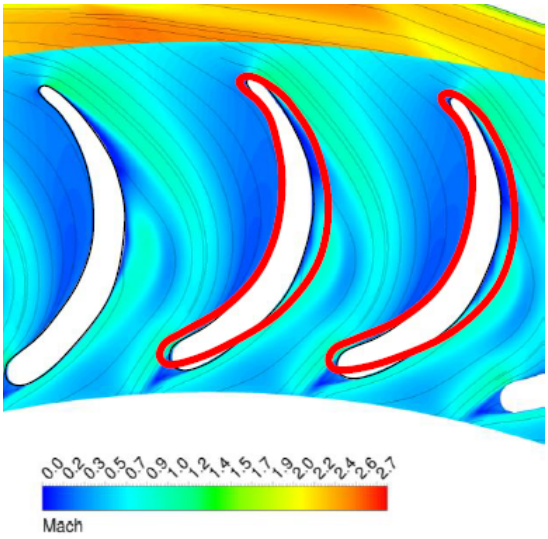

Figure 5.1: Simulated Mach number in the original rotor at shaft speed 1.1 times the original one and suggested thickness redesign (in red), [1]

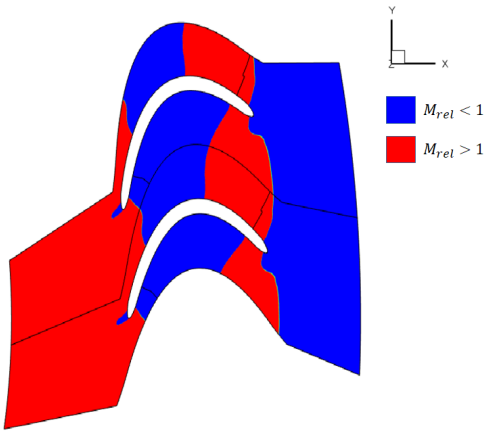

(a) Relative Mach number in the original rotor, [19]

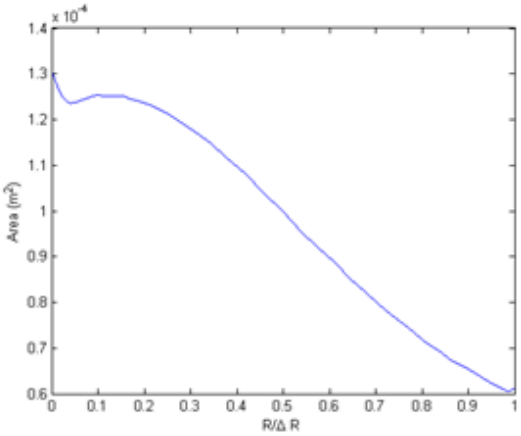

(b) area distribution of old rotor, [19]

5.0.2. PRELIMINARY DESIGN

As explained in Chapter 4, the preliminary design aims to determine the velocity triangles and an initial approximation of the rotor inlet and outlet cross sectional area (which is corrected during the detailed design). In the current section, an initial analysis is presented to determine the speed of rotation, the rotor inlet pressure and radius. Some considerations are made with respect to the flow (whether if to have a transonic or supersonic design) and the parameters are chosen in order to better meet the flow requirements. The outlet flow angle is chosen to maximize the turbine power output. After the initial analysis, the preliminary design in terms of velocity triangles and cross section areas is carried out.

INITIAL ANALYSIS

The initial analysis is started by setting the type of flow through the rotor. In fact, the turbine rotor can hypothetically be either subsonic or transonic, which from a design point of view implies a crucial difference in determining or not a throat. Depending on the variation, the existing Triogen turbines were measured to have either a subsonic or a slightly supersonic flow at the rotor inlet [19]. The aim of the redesign is to reduce entropy losses as much as possible and it was considered that a supersonic inlet always implies a leading edge shock, which reflects downstream along the nozzle and leads to consistent entropy losses. Therefore, for a better design a supersonic inlet was excluded.

Table 5.1: Range of operating conditions and blade geometries covered by different versions of Triogen's turbine

Operating conditions	Inlet total temperature	$T_{tot,2}$	[K]	560-600
	Inlet total pressure	$P_{tot,2}$	[bar]	20-35
	Mass flow	$\dot{m}$	[kg/s]	1.20-1.60
	Degree of reaction	Λ	[-]	0.26-0.475
	Shaft speed	ω	[Hz]	420-490
Geometry parameters	Inlet radius	R_2	[m]	0.11-0.12
	Outlet radius	R_3	[m]	0.07-0.08
	Stator outlet blade angle	$\alpha_{b,2}$	[deg]	-
	Rotor inlet blade angle	$\beta_{b,2}$	[deg]	-
	Rotor outlet blade angle	$\beta_{b,3}$	[deg]	-
	Rotor inlet blade height	$h_{b,2}$	[m]	-
	Rotor outlet blade height	$h_{b,3}$	[m]	-

After setting the rotor inlet conditions as subsonic, an analysis was carried out to evaluate how to better obtain such conditions. The role of each parameter in determining the relative Mach number was quantitatively evaluated through ideal gas equations, which help to visualize the relations in between thermodynamic quantities. The conclusions were afterwards extend also to the real gas case. In Chapter 2 it was explained that supersonic conditions at any location are achieved when the pressure ratio in between the local total and static pressure is grater than a critical one p_{tot}/p^*. Therefore, the relative Mach number at the rotor inlet is evaluated by means of Eq.(5.1)-(5.3). Since the rotor is taken into account, all equations have to be evaluated in the rotating frame of reference:

$$\frac{p_{tot,rel}}{p} = \left(\frac{T_{tot,rel}}{T}\right)^{\frac{\gamma}{\gamma-1}} \gtrless \frac{p_{tot}}{p*}, \tag{5.1}$$

$$T_{tot,rel} = \frac{H_{tot,rel}}{c_p}, \tag{5.2}$$

$$H_{tot,rel} = h + \frac{1}{2}w^2. \tag{5.3}$$

It is noticed that the total to static pressure ratio is linked to the total to static temperature ratio. In order to reduce the ratio $P_{tot,rel}/p$ two different paths can be followed either increasing the temperature T or reducing the total temperature $T_{tot,rel}$. If the static temperature increases, also the enthalpy h in Eq. (5.3) increases, leading to a higher value of $H_{tot,rel}$ and $T_{tot,rel}$. However, due to the fraction by c_p in Eq. (5.3) the static temperature increases more that the total one, implying in fact a lower Mach number. If the entropy s is constant, a rise in temperature corresponds to a rise in pressure. If the focus is set in reducing the total temperature by leaving the static temperature unchanged, the relative flow speed w needs to decrease. Fig. (5.3) shows that by keeping constant the flow angle α_2 (because imposed by the stator), there are three different ways of changing the velocity w: to change the speed of rotation ω, the inlet radius R_2 or to decrease the magnitude of v. The first two possibilities are consequence of a different peripheral speed u, while the third is achieved by changing again the inlet pressure p_2. Therefore, through Eq. (5.3)-(5.1) it was observed that the total to static pressure ratio (and consequently the flow Mach number) depends on the rotor inlet pressure p_2 and on the relative velocity w_2. Subsonic conditions are reached for high values of p_2, for low values of w_2 or by a combination of the two.

By looking at Eq. (2.9) it is clear that for an isentropic expansion, a higher pressure p_2 implies a higher degree of reaction. It is concluded that the flow relative Mach number at the rotor inlet can be controlled by:

- Degree of reaction Λ
- Speed of rotation ω
- Rotor inlet radius R

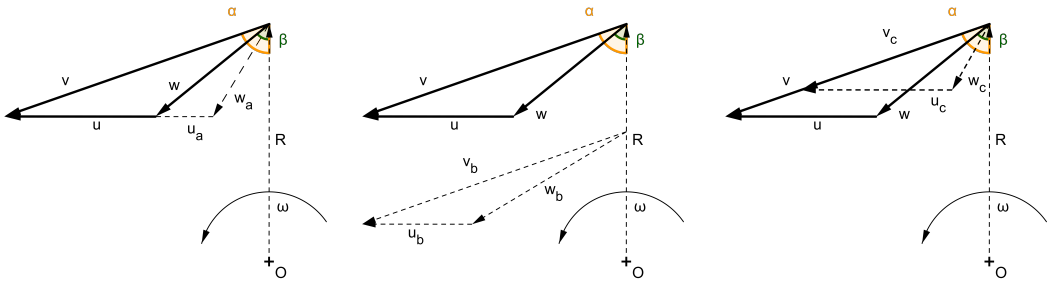

(a) Effect of the shaft speed ω (b) Effect of raidus R (c) Effect of the pressure p

Figure 5.3: Velocity triangles depending on the shaft speed, on the radius and on the pressure

In between the three possibilities, the best one would be to change only the speed of rotation. This, in fact, would have a minor impact on the overall system, while changing the degree of reaction or the inlet radius implies a redesign of the stator as well. An analysis was done to determine which parameters to change. A target inlet Mach number was set to $M_{2,rel} = 0.8$; the choice of this value is due to the fact that the turbine often works in off design conditions, therefore the design point cannot be too close to transonic conditions. On the other hand, a strongly subsonic flow at the rotor inlet would lead to steep area variations due to the higher expansion ratio that has to occur in the same nozzle length $R_2 - R_3$.

The focus was set on the influence of the speed of rotation. The radius was kept at the original design value and it was assumed a degree of reaction of $\Lambda = 0$. It was calculated that in order to achieve the target inlet Mach number, the shaft speed should be multiplied by a factor of 2 with respect to the original speed. Variants with respect to the original design running with higher shaft speeds exist, however the calculated one goes far beyond the material's capabilities and bearing loads, due to the high inertia forces that it would imply. Therefore, the possibility of simply increasing the speed of rotation was discarded.

Afterwards, an analysis was done on the effects of variations of pressure and inlet radius, represented in Fig.(5.4). Again it was set as a target the inlet Mach number $M_{2,rel} = 0.8$, such value can be reached by increasing the inlet pressure to a value of $p_2/p_3 = 7$, or by increasing the inlet radius to approximately $R_2/R_{2,original} = 0.65$. Increasing the original radius of 65% would imply higher inertia effects, therefore this option was discarded as well.

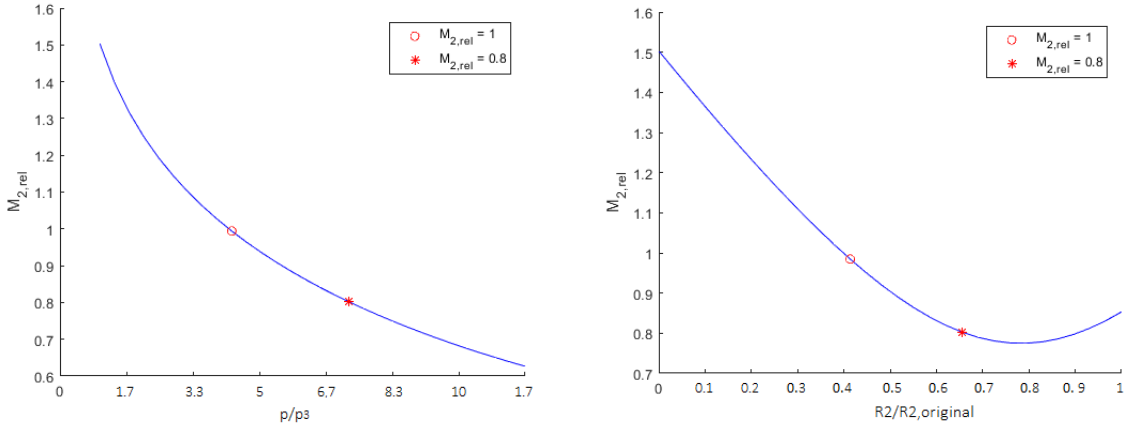

(a) $M_{2,rel}$ depending on p_2 (b) $M_{2,rel}$ depending on R_2

Figure 5.4: Mach number at the rotor inlet depending on inlet pressure and radius

It was concluded that to have a subsonic flow at the inlet of the stator it is necessary to change the degree

Table 5.2: Boundary conditions and geometry constrains for Triogen's rotor redesign

Operating conditions	Inlet total temperature	$T_{tot,2}$	[K]	580-610
	Inlet total pressure	$P_{tot,2}$	[bar]	30-35
	Outlet static pressure	p_3	[bar]	0.2-1.0
	Mass flow	$\dot{m}$	[kg/s]	1.5-2.0
	Degree of reaction	Λ	[-]	0.5
	Shaft speed	N	[Hz]	450-50
Geometry parameters	Inlet radius	R_2	[m]	-
	Outlet radius	R_3	[m]	-
	Stator outlet blade angle	$\alpha_{b,2}$	[deg]	-
	Outlet flow angle	α_2	[deg]	0.1

of reaction. For the speed of rotation specified in the most recent turbine version, $M_{2,rel} = 0.8$ is reached for $p_2/p_3 = 7$. In the current case the inlet pressure was set to $p_2/p_3 = 8.3$, the choice of this pressure rather than a lower one is related to the detailed blade design and will be explained further in the chapter. At such inlet condition the degree of reaction was set to $\Lambda = 0.5$. Changing the value of Λ implies a redesign of the stator, since a different outlet area is needed to expand to a higher pressure. However, because of the overall optimization process the turbine is going thought, this was not considered to be a major issue.

After determining pressure p_2 at the inlet of the rotor, the only parameter left to determine in the preliminary analysis is the flow direction α_3 at the rotor outlet. As discussed in Chapter 2, the turbine work extraction is maximized for a fully radial outlet flow, therefore for $\alpha_3 = 0°$. However, in the current case it was set $\alpha_3 = 0.1°$ because of numerical reasons. In the code used, an angle of 0.0° implied some fractions divided by 0 in evaluating the velocity triangles.

Finally, the full set of boundary conditions is defined, as listed in Tab. (5.2). For the operating conditions it is given a range rather than the exact values and geometrical parameters are not specified to preserve the company's confidentiality.

One-dimensional design

The one-dimensional analysis is done to determine the velocity triangles and a first approximation of the cross sectional area at the rotor inlet and outlet. In this section, the procedure described in Chapter (4.1) is followed step by step: the rotor inlet and outlet conditions are set by means of an isentropic expansion. All thermodynamic properties are calculated by means of rothalpy and entropy conservation and finally, by means of mass conservation, a first approximation of cross sectional area is calculated. The entropy level is set according to the total conditions. The outputs of the analysis are reported in Tab. (5.3), while in Fig. (5.4) are represented the velocity triangles.

At the inlet the flow in the absolute frame of reference is highly supersonic, while it is subsonic in the relative, confirming that the right inlet boundary conditions were provided. At the outlet, the flow in the relative frame of reference is accelerated, $w_3 > w_2$, while is decelerated in the the absolute frame of reference, $v_3 < v_2$. The absolute velocity v_3 is still high, when ideally a zero velocity would be preferable. However, at the exit the speeds w_3 and u_3 are fixed, while the angle α_3 is specified by design. As shown in Fig. (5.5), to further decelerate the absolute flow, the angle α_3 should be negative and the velocity w_3 should shift towards a radial direction (from triangle (v_a, w_a, u) to triangle (v_b, w_b, u) in figure). In the CFD simulations ran by Harink et Al. [1] it was noticed that the exit angle α_3 had a grater influence than the speed v_3 on the overall rotor efficiency, therefore the angle was left unchanged.

5.0.3. Detailed blade design

The detailed blade design is carried out following all steps of Section 4.2, which makes sure that the blade has physical dimensions and that the blade passage is dimensioned according to the boundary conditions. The blade is built by means of 14 different parameters; most of them where arbitrarily chosen at the beginning to set a blade frame and were left unchanged during the design process. The proper design was reached by iteratively changing only three parameters: the stagger angle (δ), the location of maximum thickness along

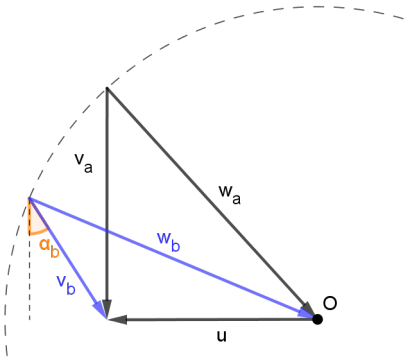

Figure 5.5: Dependence of velocity v on the angle α

Table 5.3: Absolute and relative Mach number at the rotor inlet/outlet

		Location 2	Location 3
M	[-]	2.18	1.43
M_{rel}	[-]	0.75	1.95

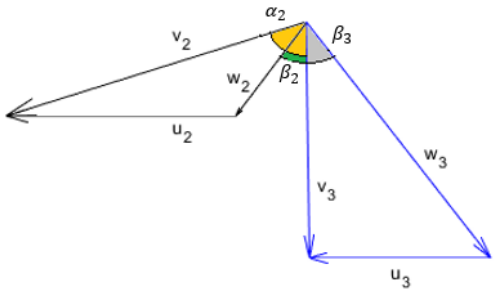

Table 5.4: Inlet/outlet velocity triangles

the blade (loc_C) and the blade maximum thickness (th_C).

The first parameter to be set was the stagger angle δ. A sensitivity analysis was performed for the stagger angle, in Fig. (5.7) are represented two possible blade design, one for $\delta = -1°$ and one for $\delta = -4°$. Two main conclusions were drawn on the blade curvature, Fig. (5.7a), and on the distance d in between blades along the nozzle, Fig. (5.7b):

- by moving from slightly negative to more negative angles, the distance in between blades increases at the inlet and decreases at the outlet;
- by moving from slightly negative to more negative angles, the blade curvature increases.

It was mentioned that through CFD simulations on the original rotor design, flow separation was noticed on the pressure side of the blade. This was imputed also to the excessive blade curvature [1]. Therefore, a positive or slightly negative stagger angle is preferable over more negative ones. Such choice has an effect also on the blade height, defined as $h_{b,2} = A_2^* / d_2$ in Eq. (4.28). Being the value of A_2^* imposed, the blade height $h_{b,2}$ depends on the distance d_2. Therefore, $h_{b,2}$ necessarily decreases moving from positive towards negative stagger angles. Looking at the first approximation inlet area A_2, calculated during the preliminary design, it can be seen that at the given inlet pressure p_2, the inlet cross sectional area is of the order of $10^{-5} m^2$. This implies an inlet blade height in the order of $10^{-3} m$, which leads to problems related to the boundary layer. In fact, if viscosity is taken into account a boundary layer is developed. If the blade height and the boundary layer thickness are of a similar order of magnitude, the overall cross sectional area is be affected. A negative stagger angle contributes keeping the blade height as high as possible. Given the previous explanation, a positive stagger angle appears to be beneficial for the blade design. However it was noticed that, for the given parametrization, the value of δ also influences the maximum blade thickness. Negative stagger angles allow thicker blades; to reach a physical throat for positive stagger angles, the blade thickness has to be sensibly

lower. In the current case, a positive value of δ implied a lower blade thickness compared to the original one, while Harinck et Al. [1] suggested to increase the thickness in order to avoid flow separation. For all these reasons, the stagger angle was set to a value of $\delta = -1$. The influence of the stagger angle on the blade shape is resumed in Fig. (5.6).

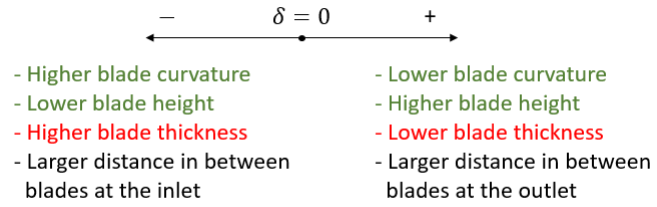

Figure 5.6: Influence of the stagger angle on the blade design

The choice of the pressure $p_2/p_3 = 8.3$ in the preliminary design is related as well to the blade curvature and thickness. The inlet pressure sets the rothalpy level, which is used to calculate the sonic line of the nozzle. For lower inlet pressures, the sonic line is higher, meaning that at each location along the nozzle a physical throat is reached for larger cross sectional areas compared to higher inlet pressures. The concept can be better understood by looking at Fig. (5.8): the sonic line and the area distribution along the nozzle are plotted for $p_2/p_3 = 8.3$ and $p_2/p_3 = 7$, the stagger angle and blade thickness are constant in the two cases. It is evident that for $p_2/p_3 = 7$ the area distribution is below the sonic line, meaning that an isentropic expansion cannot be reached. The area distribution can be fixed by:

1. increasing the distance in between blades. This can be achieved by setting the stagger angle to more negative values, which implies a strong blade curvature and a lower blade height at the inlet;

2. reducing the blade thickness.

Recommendations made from Harinck et Al. [1] suggested to increase the blade thickness and decrease the blade curvature. Therefore, none of the two options was considered as valuable and the inlet pressure was set to a higher value.

Once the stagger angle δ was fixed, the maximum blade thickness th_C and its location loc_C were iteratively changed to obtain an area distribution that touches the sonic line in one location, providing therefore a physical throat.

5.0.4. Blade parametrization discussion

The final shape achieved through the detailed design is represented in Fig. (5.9), the aspect ratio of the geometry was changed. In Tab. (5.5) is reported the percentage difference in between the area obtained at the rotor inlet/outlet through the parametrization and the imposed target area (A_2^* and A_3^*). It is also reported the difference between the area obtained at the throat and the theoretical throat area described by the sonic line. It is noticed that no sudden changes in slope or concavity occur both in the nozzle cross sectional area or in the blade height, Fig. (5.9a)-(5.9b). In terms of cross sectional area, the largest changes in slope are noticed in proximity of the leading and trailing edge, however such changes cannot be avoided due to the shape of the blade. The area distribution is always above the sonic line, Fig. (5.9c), and touches the sonic line in one single point in order to provide a physical throat. In the current case, the physical throat corresponds also to a geometrical one, no other area local minima are present along the mid line Ψ. The nozzle inlet and outlet area are matched with an error of respectively 0.00% and −0.41%, while the deviation of the throat area from the sonic line is of 0.09%. Therefore, the blade parametrization proved itself as capable of satisfying the design requirements.

The blade shape is compared to the original one. The provided blade is thicker and with a lower curvature, as suggested by Harinck at Al. [1]. The inlet and outlet blade angles match the flow direction and are designed for a higher shaft speed that the original rotor. However, the inlet blade height is approximately one

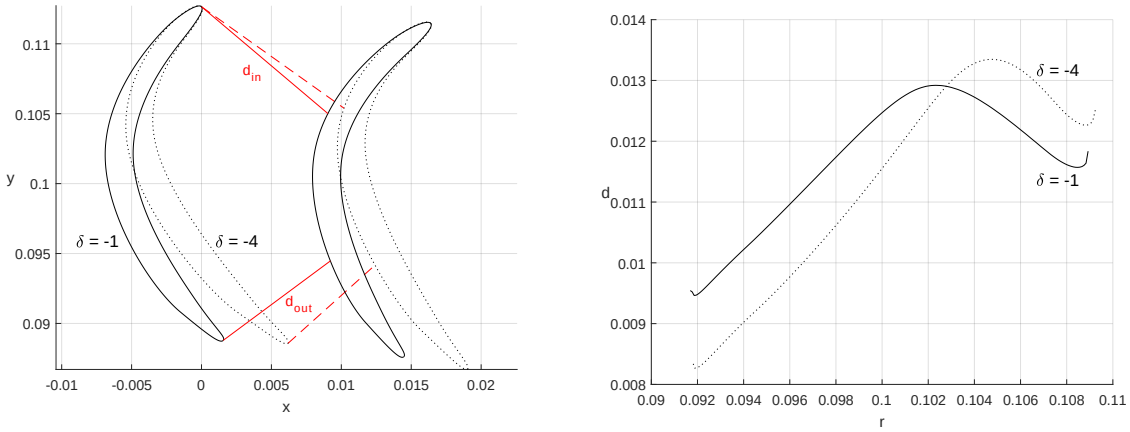

(a) Blade curvature and inlet/outlet distance in between blades

(b) Distance in between blades

Figure 5.7: Effects of stagger angle δ on the blade curvature and on the distance in between blades

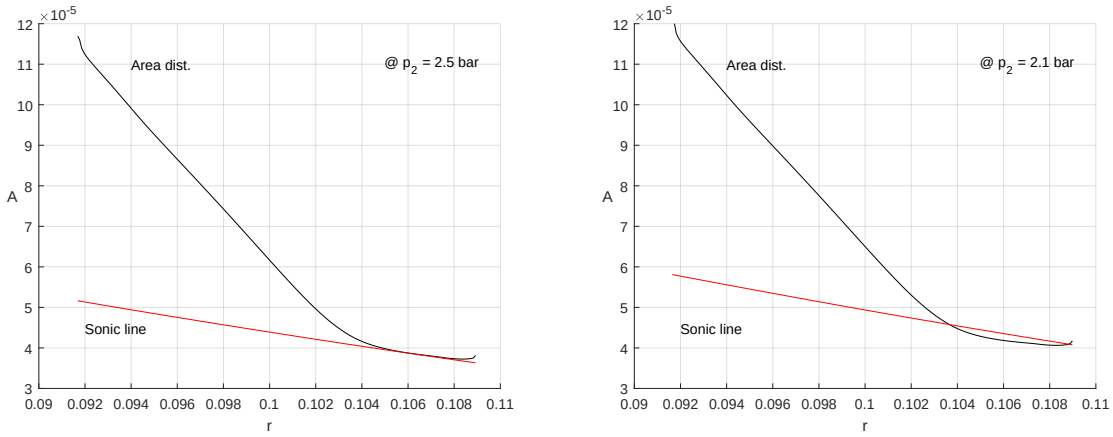

(a) Inlet pressure $p_2/p_3 = 8.3$

(b) Inlet pressure $p_2/p_3 = 7$

Figure 5.8: Influence of inlet pressure on the sonic line and area distribution at constant stagger angle and blade thickness

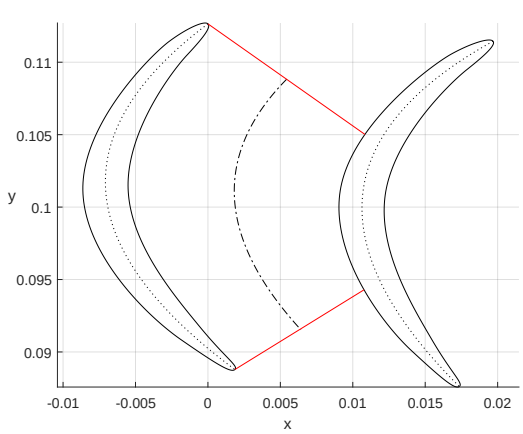

(a) Blade cross section, frame of reference (x,y)

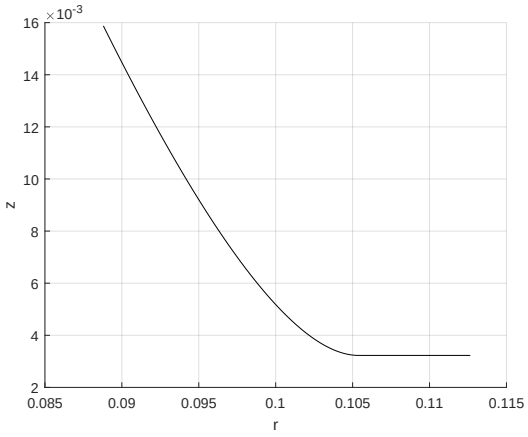

(b) Blade height, frame of reference (r,z)

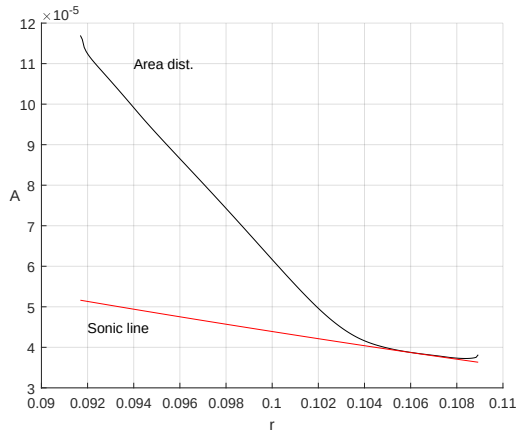

(c) Area distribution along the mid line Ψ

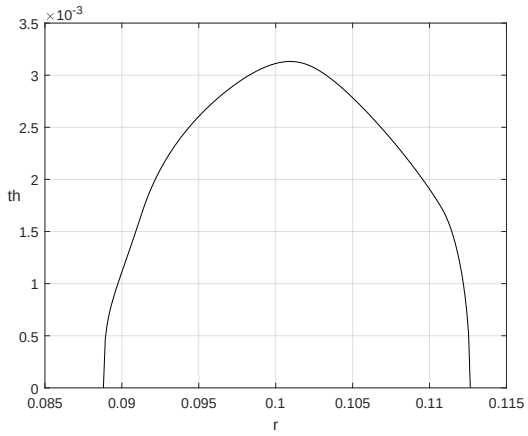

(d) Blade thickness

Figure 5.9: Final blade design

third compared to the original one, the reached value is considered to be too low to be actually implemented in a turbine. In a real case, in fact, the boundary layer development affects the cross sectional area, as explained in Section 5.0.3.

5.0.5. Evaluation of three dimensional effects

The blade design methodology proposed in the current master thesis relies on a one dimensional approximation to generate a three dimensional shape. Therefore, the current section aims to verify what is the influence of such approximation on the final result. To do so, the flow in between two blades is evaluated by means of computational fluid dynamics (CFD); the shape used is the one determined in Section 5.0.3 and the simulation is ran using an in-house code developed at Stanford University by Pecnik et Al. [31]. At first, general comments are given on the results of the simulation, afterwards results are compared to the expected ones.

The CFD simulation was ran by using a quasi-3D mesh. To do so, a 2D mesh of the nozzle was created in

Table 5.5: Final blade dimensions and deviations from the imposed geometry

Area deviation	err_{A2}	[%]	0.00
	err_{A3}	[%]	-0.41
Throat deviation from sonic line	$\text{err}_{A,th}$	[%]	0.09

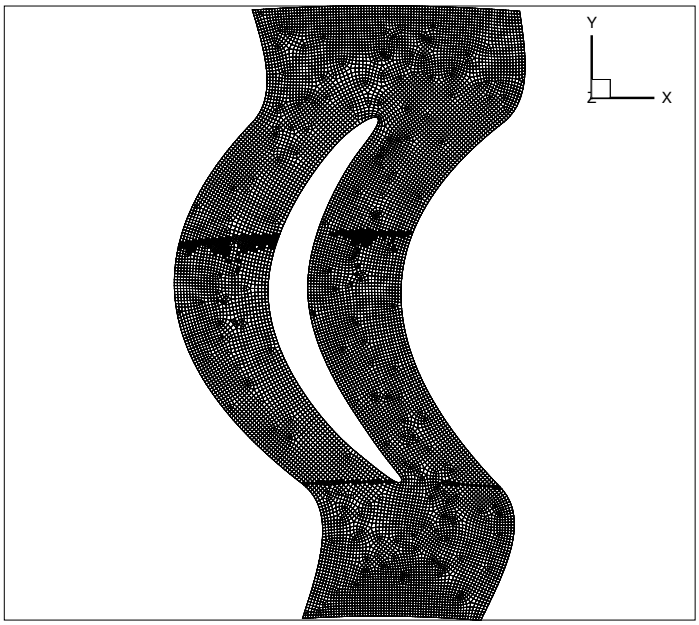

Figure 5.10: Quasi-2D nozzle mesh

the plane (x, y) and was afterwards extruded to create the blade height; the twoo dimensional mesh is shown in Fig. (5.10). A quasi-3D mesh keeps into account the area variations along the nozzle, however the velocity vectors have no z component, therefore $\bar{v} = (\bar{v}_x, \bar{v}_y)$. The CFD simulation was ran by G. Otero with a second order accuracy in space, using a multiparameter equation of state for the working fluid [5]. The simulation was ran until the residuals dropped to the order of 10^{-6}. Results for pressure p, relative Mach number M_{rel}, the relative velocity component w_y and the absolute value of the pressure gradient $gradP$ are reported in Fig. (5.11), where the aspect ratio of the blades was modified.

By looking at the pressure, Fig. (5.11a), it is noticed that the flow conditions at the inlet and outlet of the nozzle vary consistently moving form the suction side of one blade to the suction side of adjacent one. Therefore, it is impossible to uniquely define the inlet/outlet conditions of the nozzle. The flow initially expands smoothly, but in the second part of the nozzle two sudden recompressions occur, one in proximity of the blade suction side and the other one in proximity of the blade pressure side. The first one is an oblique shock, as demonstrated by pressure gradient plot in Fig. (5.11d). The second one might be related as well to a shock, however the velocity component w_y in Fig. (5.11c) shows some recirculation of the flow on the pressure side of the blade. At that location it is noticed flow separation and recirculation, which is not expected in an inviscid simulation. Such flow behaviour was imputed to numerical diffusion, which due to a too coarse mesh introduces some fictitious viscosity in the system. Therefore, the flow recompression was not linked to a real shock occurring in the nozzle. In Fig. (5.11b) are displayed the regions of the nozzle in which the flow in the relative frame of reference is subsonic and supersonic; the transition line is positioned in the first part of the nozzle. A transition to subsonic flow occurs also on a small region on the blade suction side, immediately after the oblique shock, and in the recirculation zone. If Fig. (5.12b) is compared to Fig. (5.2a) it is noticed that in the original rotor operating at higher speeds, a strong shock wave forces the flow at the rotor exit to subsonic conditions in the relative frame. In the current design the oblique shock previously described has minor effects on the flow. However, for a fair comparison the proposed blade shape should be evaluated coupled to the stator.

After giving general comments on the CFD simulation results, the flow properties along the mid line Ψ (for Ψ refer to Fig. (5.9c)) were extrapolated and compared to the results of the 1D case; the latter were calculated by means of the analytic solution method. In Section 3.5 it was explained that the use of the analytic solution method is recommended for inverse engineering, while the flow propertied through a given geometry should be calculated by means of the finite differences solver. However, the FDS code was implemented only for ideal gas, while the test case design was done using toluene as a working fluid. Therefore, ASM was used for

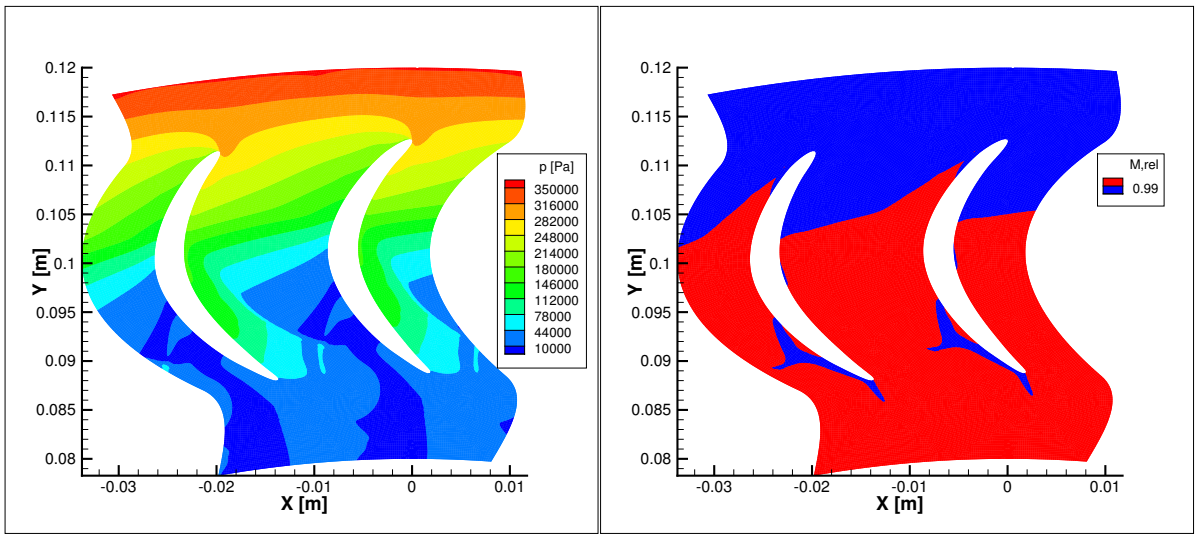

(a) Static pressure

(b) Relative Mach number

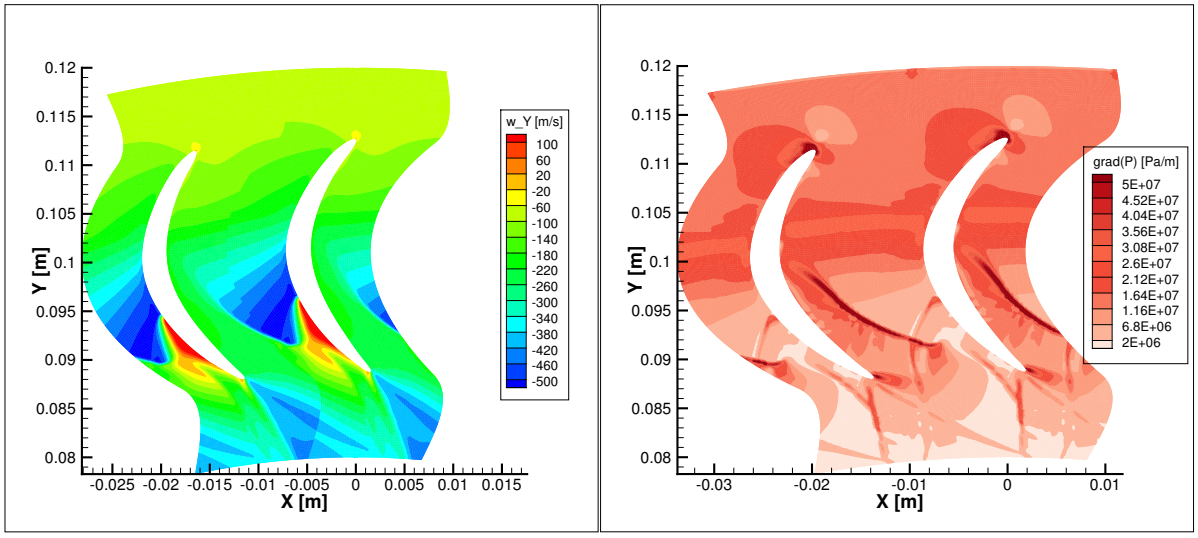

(c) Velocity component w_y

(d) Pressure gradient

Figure 5.11: CFD simulation of the flow wield through the blade passage

Table 5.6: Percentage difference between imposed boundary conditions and achieved values

	% diff	
	Inlet	Outlet
w	-2.00	36.86
M_{rel}	-2.00	38.41
p	14.57	-43.93
$\dot{m}$	-22.51	
r_{th}	0.663	

the design mass flow, while for rothalpy and entropy were used the values calculated in Section 5.0.2. In Fig. (5.12a)-(5.12c) are plotted the values of relative velocity, relative Mach number and static pressure along the mid line; results are reported both for ASM and CFD simulation. All values along each curve are divided by the inlet value calculated by ASM. In Fig. (5.12d) is plotted the percentage difference in between the two solvers for each of the variables previously mentioned. In Tab. (5.6) are reported the percentage differences of each variable at the inlet and outlet of the nozzle, the percentage difference for the mass flow and for the throat location along Ψ. The mass flow of the CFD simulation was calculated by taking into account the velocity component w_y through the cross sectional area in the plane (x,z) at the nozzle inlet:

$$\dot{m} = -\int \rho(x) w_y(x) h_{b,2} dx. \tag{5.4}$$

By looking at Fig. (5.12) it is clear that a consistent difference exists in between the solutions form ASM and CFD, however the trends of the two simulations are similar. The focus is initially set on the relative velocity and relative Mach number plots: the percentage difference in between ASM and CFD is of 2% at the inlet and it is always below 10% till the radius $R = 0.1m$ is reached. Afterwards the flow speed calculated by CFD increases very rapidly and suddenly drops due to a shock wave, while the ASM solutions keeps on increasing smoothly. The relative Mach number follows the same trend of the relative velocity. The difference in between the two solutions might be linked to two different factors. First of all, the fast increase of w in the CFD simulation might be a consequence of the numerically generated diffusion. In fact, due to separation the cross sectional area of the nozzle is reduced and the flow accelerates. In addition, a one dimensional model is sensible to normal shock waves but blind to oblique ones. Since the nozzle was designed through a 1D approximation, the design could not predict and therefore avoid oblique shock waves. While the percentage difference of relative velocity and relative Mach number is comparable, the percentage difference of pressure along the nozzle is always higher if compared to the the other variables. This was linked to the fact that the mass flow determined by choked conditions in the 3D geometry is 22% lower than the design one, as reported in Tab. (5.6). Mass flow is an integral quantity, depending on the velocity and density distribution along the cross section. In the 3D case the velocity variation along the cross section is too high to be approximated with one single value (as in the 1D case). This difference leads to the mismatch in between the expected mass flow and the one obtained by the simulation. However, the model was capable of predicting accurately the physical throat location: the percentage difference in between ASM and CFD with respect to the transonic point is of 0.663%. By looking at Fig. (5.11b) it is noticed that the position of the transonic point is well predicted on the mid line but that it varies considerably moving towards the pressure and suction side. This confirms again that integral quantities, as the mass flow, are affected by 3D effects.

It is concluded that the one dimensional approximation is not capable of guaranteeing the right mass flow and inlet/outlet boundary conditions. The difference in between the predicted flow and the obtained one is due to the fact that mass flow is an integral quantity and regions far away from the mid line affect the results along the mid line as well. However, the throat location along the mid line is well predicted and the flow behaviour follows a trend in line with the expected one, meaning that a part from integral quantities, the 1D approximation could represent the flow along Ψ. Therefore, the 1D flow approximation is a starting point for adding additional other levels of complexity (as a 2D rather than 1D approximation) to achieve a final blade design.

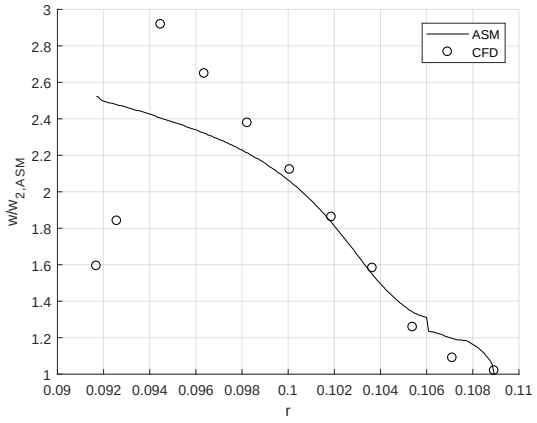

(a) Realtive velocity w

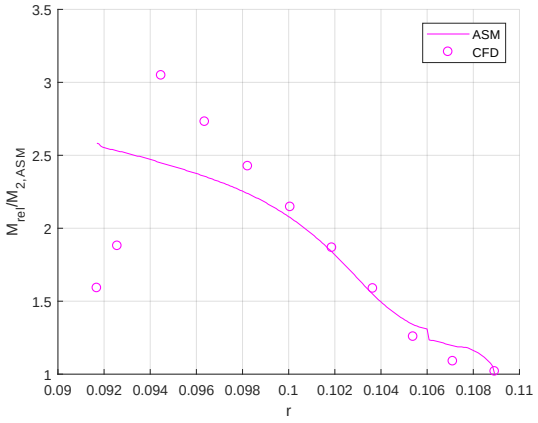

(b) Relative mach number M_{rel}

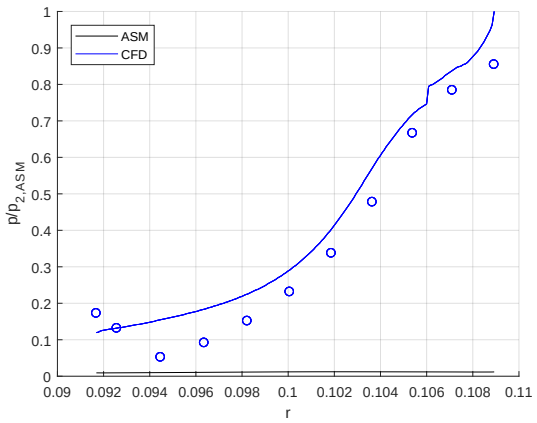

(c) Static pressure p

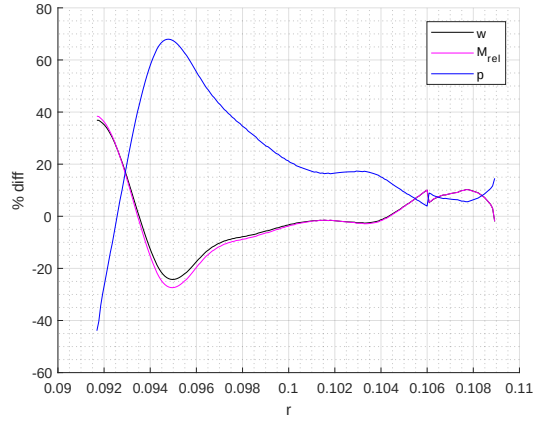

(d) Percentage differences between ASM and CFD for w, M_{rel} and p

Figure 5.12: Comparison between ASM and CFD along the nozzle mid line

6

CONCLUSIONS AND RECOMMENDATIONS

The goal of the master thesis was to build a design methodology for rotor blades of an Organic Rankine cycle inflow turbine, with transonic flow, real gas effects and in a radial inflow configuration. An inverse design approach was used: the focus was set on the blade passage and on the design of a proper nozzle. Due to the lack of literature on the expansion of transonic flows in a rotating frame of reference, the thesis first focused on deriving relations on choked conditions and flow properties in a one dimensional flow through an isentropic nozzle. The conclusions of the study were used to build a blade design methodology; the last step was to use the methodology to suggest a new design for Triogen's turbine. The theory developed on one dimensional, rotating nozzles and the blade design methodology were discussed separately.

6.1. 1D ANALYSIS OF ROTATING NOZZLE WITH CENTRIPETAL FLOW

An analysis was done on a one dimensional, isentropic, centripetal flow expanding thought a rotating nozzle. It was already known that if a nozzle is put in rotation, the transonic point moves downstream with respect to the geometrical throat. However, the influence of the shape of the nozzle on the overall flow conditions was unknown. The aim of the study was to determine analytically where choked conditions occur and to be able to control that position. In addition, it was looked for an analogy with the static nozzle case (where the flow only depends on total condition and on the ratio A/A_{th}) to link the flow conditions along the nozzle only to the area and to other superimposed quantities, which turned out to be rothalpy, entropy and peripheral speed.

In contrast to nozzles in stationary frame of reference, it was found that a centripetal subsonic flow in a rotating nozzle can accelerate even in the diverging part of the nozzle. It is concluded that the transonic point is not always located downstream with respect to a geometrical throat (as previously thought) and it can be designed to coincide with the geometrical throat. In addition, a geometrical throat is actually not needed in a rotating nozzle.

Chocked conditions were discussed for a nozzle with specified inlet and outlet radius, mass flow, rothalpy and speed of rotation were set. It was verified that the model only considers isentropic solutions for cross sectional areas larger that a minimum one, at which the flow is choked. The minimum area represents a physical throat and it is different at each location along the nozzle, therefore $A_{th} = A(I, \dot{m}, s, \omega, R)$. By plotting the throat area at each radius in the plare (r, A) (for imposed values of I, $\dot{m}$, s and ω), it was possible to draw a sonic line, which was proved to be a valid method for inverse nozzle design. If the area distribution along a nozzle ($A = A(r)$) intersects the sonic line, a physical throat is provided. It was understood that a physical throat can be set to any location along a nozzle, but its location influences the required cross sectional area; this represents a main difference compared to static nozzles. The sonic line proved itself to be a valid tool for inverse nozzle design. It was also concluded that for a nozzle with a given geometry and given values of rothalpy, entropy and speed of rotation, choked conditions are uniquely defined. In addition, the flow conditions along the nozzle can be analytically calculated. A graphical methodology was provided to determine flow conditions along the nozzle, methodology that can be also used for inverse engineering.

6.2. BLADE DESIGN METHODOLOGY

The rotor blade design methodology developed in the current work consists of creating a nozzle in the blade passage. The flow is approximated as one dimensional and isentropic, therefore the nozzle throat is provided according to the sonic line in the (r, A) plane. The inlet and outlet area are specified as well to respect pressure and velocity boundary conditions. The blade shape is obtained by means of a blade parametrization, that ensures that geometrical constrains as thickness and blade concavity are respected.

The blade parametrization implemented is capable of creating a 3D by assigning an area distribution around the nozzle mid line. Ty he parametrization was able to precisely provide the specified cross sectional area at the inlet, throat and outlet. The constrains on the blade shape are respected, as no changes is concavity along the camber line and the blade height.

The flow field of the design blade was evaluated by means of a three dimensional CFD simulation. When the 3D effects are taken into account, the velocity and thermodynamic properties consistently change from the suction side to the pressure side of two adjacent blades, while through the 1D approximation they are assumed to be constant at each location along the mid line. Such difference makes impossible to predict accurately integral quantities, as the mass flow. The values of relative velocity, relative Mach number and static pressure were evaluated along the nozzle mid line and compared to the analytic results of a 1D flow through the same nozzle. It is recalled that the blade shape is designed based on a 1D approximation, so the analytic solution to the 1D flow represents the target flow field. The trend of relative velocity, relative Mach number and static pressure along the nozzle mid line are similar, meaning that the area distribution assigned to the nozzle is a good starting point for a final design. However, the values of the mentioned quantities were predicted with a consistent error due to the mass flow, different from design. An oblique shock wave occurs on the blade pressure side in the second part of the nozzle; oblique shock waves are determined by 2D effects and cannot be predicted by 1D flows, so the design methodology is incapable of predicting this kind of discontinuity.

It is concluded that a one dimensional flow is an approximation for the design a three dimensional geometry. In fact, the regions close to the nozzle walls are not well represented by the mid line. However, the right trend in proximity of the mid line confirms that the flow physics were understood and that introducing new levels of complexity (as 2D flow approximation rather than 1D) will lead to a more accurate design. Therefore, the work presented is a good starting point for a more complex and complete blade design methodology with inverse design approach.

6.3. RECOMMENDATIONS

The blade design methodology proposed is entirely based on the relations derived on a one dimensional, isentropic, centripetal flow. Validation of the derived relations for ideal gas was carried out by comparison with a finite volume solver (FVS), which was not correctly implemented for real gas. Therefore, it is necessary to adapt the FVS for real gas to prove if the relations derived are independent on the gas equation of state.

The one dimensional approximation proved itself to be valid in determining the throat location and the trend of the flow properties along the nozzle. It failed in determining integral quantities. A more flexible blade parametrization could be introduced, allowing to iteratively change the blade shape by keeping as a target the throat area and location. If the flow field is solved at each iteration, more uniform properties can be reached at the nozzle cross section, which allows for a better prediction of the integral quantities. In addition, the one dimensional flow approximation is incapable of predicting shock waves, which could be taken into account either passing to a 2D or 3D model or by iteration of the nozzle geometry.

The current design was carried out using the fluid properties at the stator outlet as an input for the rotor. However, the two were not coupled and their interaction might lead to different results. Therefore, the two components should be integrated to obtain a full turbine stage design.

Finally, the whole design was carried out under several assumptions. In particular, viscous effects were neglected. These play an important role in determining the flow through the turbine blades, so for a final design viscosity should be introduced in the model.

BIBLIOGRAPHY

[1] J. Harinck, R. Pecnik, and P. Colonna, *Three-Dimensional RANS Simulation of a High-Speed Organic Rankine Cycle Turbine,* , 1 (2012).

[2] A. Vaughan, *Paris climate deal: key points at a glance,* https://www.theguardian.com/environment/2015/dec/12/paris-climate-deal-key-points, accessed: 12-12-2016.

[3] *2030 energy strategy,* http://ec.europa.eu/energy/en/topics/energy-strategy-and-energy-union/2030-energy-strategy, accessed: 15-09-2017.

[4] L. Balling, *Flexible future for combined cycle,* Modern Power Systems **30**, 61 (2010).

[5] G. J. O. Rodriguez, *Master of Science Thesis, Mechanical Engineering, TU Delft*, Ph.D. thesis (2014).

[6] *Triogen - company,* http://www.triogen.nl/about/company, accessed: 16-10-2017.

[7] S. Quoilin, M. V. D. Broek, S. Declaye, P. Dewallef, and V. Lemort, *Techno-economic survey of Organic Rankine Cycle (ORC) systems,* Renewable and Sustainable Energy Reviews **22**, 168 (2013).

[8] Y. Li and X.-d. Ren, *Investigation of the organic Rankine cycle (ORC) system and the radial-inflow turbine design,* Applied Thermal Engineering **96**, 547 (2016).

[9] B. Dong, G. Xu, X. Luo, L. Zhuang, and Y. Quan, *Analysis of the supercritical organic Rankine cycle and the radial turbine design for high temperature applications,* Applied Thermal Engineering **123**, 1523 (2017).

[10] M. Zangeneh, *A compressible three???dimensional design method for radial and mixed flow turbomachinery blades,* International Journal for Numerical Methods in Fluids **13**, 599 (1991).

[11] O. O. and M. J E, *Lifting surface theory of axial compressor blade rows. i - subsonic compressor. ii - transonic compressor,* AJAA (1974), 10.1016/j.applthermaleng.2015.12.009.

[12] A. d. O. Falcão, *Lifting-surface theory of straight cascades of swept blades,* International Journal of Mechanical Sciences **18**, 313 (1976).

[13] C. Tan, W. Hawthorne, J. McCune, and C. Wang, *Theory of blade design for large deflections: Part ii—annular cascades,* Journal of Engineering for Gas Turbines and Power **106**, 354 (1984).

[14] J. E. Borges, *A three-dimensional inverse method for turbomachinery: Part i—theory,* Journal of Turbomachinery **112**, 346 (1990).

[15] W. Ghaly and C. Tan, *A parametric study of radial turbomachinery blade design in three-dimensional subsonic flow,* ASME paper 89-GT **84** (1989).

[16] M. Lighthill, *A new method of two-dimensional aerodynamics design,* in *R&M1111, Aeronautical Research Council* (Citeseer, 1945).

[17] S. Dixon and C. Hall, *Fluid Mechanics and Thermodynamics of Turbomachinery,* Fluid Mechanics and Thermodynamics of Turbomachinery , 1 (2010), arXiv:arXiv:1011.1669v3 .

[18] N. Anand, *Master of Science Thesis, Mechanical Engineering, TU Delft*, Ph.D. thesis (2016).

[19] G. Otero Rodriguez, *Insight of the Original Tri-O-Gen Turbine,* (2015).

[20] J. P. Buijtenen, W. P. Visser, T. Tinga, S. Shakariyants, and F. Montella, *Gas Turbines*, edited by J. Singh (2007).

[21] Ansys Fluent, *Continuity and Momentum Equations,* (2006).

[22] C. Wu, *Thermodynamics and heat powered cycles: a cognitive engineering approach* (Nova Publishers, 2007).

[23] I. Ansys, *Equations for a Rotating Reference Frame,* (2009).

[24] P. K. Kundu, I. M. Cohen, and D. R. Dowling, *Academic Press 4th ed* (2012) p. 891, arXiv:1003.3921v1 .

[25] Aerospace Engineering, *Supersonic Aerodynamics: Designing Rocket Nozzles,* (2016).

[26] P. Bakker and B. van Leer, *Lecture notes on Gasdynamics, AE4-140* (2005).

[27] M. J. Zucrow and J. D. Hoffman, *Gas Synamics, Volume 1* (1976).

[28] J. D. Anderson, *modern compressible flow, with historical prospective*, edited by McGraw - Hills (1982).

[29] NASA, *Oblique Schock Wave,* (2015).

[30] M.-S. Liou, *A sequel to ausm: Ausm+,* Journal of computational Physics **129**, 364 (1996).

[31] R. Pecnik, V. E. Terrapon, F. Ham, G. Iaccarino, and H. Pitsch, *Reynolds-averaged navier-stokes simulations of the hyshot ii scramjet,* AIAA journal **50**, 1717 (2012).